Title
Modeling Global Carbon Costs of Plant Nitrogen and Phosphorus Acquisition

Journal
Journal of Advances in Modeling Earth Systems, 14(8)

ISSN
1942-2466

Authors
Braghiere, RK
Fisher, JB
Allen, K
et al.

Publication Date
2022-08-01

DOI
10.1029/2022ms003204

Peer reviewed

JAMES | Journal of Advances in Modeling Earth Systems

RESEARCH ARTICLE
10.1029/2022MS003204

Modeling Global Carbon Costs of Plant Nitrogen and Phosphorus Acquisition

R. K. Braghiere[1,2,3], J. B. Fisher[4], K. Allen[5], E. Brzostek[6], M. Shi[7], X. Yang[8], D. M. Ricciuto[8], R. A. Fisher[9,10], Q. Zhu[11], and R. P. Phillips[12]

[1]Jet Propulsion Laboratory, California Institute of Technology, Pasadena, CA, USA, [2]Joint Institute for Regional Earth System Science and Engineering, University of California Los Angeles, Los Angeles, CA, USA, [3]Division of Geological and Planetary Sciences, California Institute of Technology, Pasadena, CA, USA, [4]Schmid College of Science and Technology, Chapman University, Orange, CA, USA, [5]Manaaki Whenua—Landcare Research, Lincoln, New Zealand, [6]Department of Biology, West Virginia University, Morgantown, WV, USA, [7]Pacific Northwest National Laboratory, Richland, WA, USA, [8]Environmental Sciences Division and Climate Change Science Institute, Oak Ridge National Laboratory, Oak Ridge, TN, USA, [9]Center for International Climate Research, Oslo, Norway, [10]Laboratoire Évolution & Diversité Biologique, CNRS:UMR, Université Paul Sabatier, Toulouse, France, [11]Climate and Ecosystem Sciences Division, Climate Sciences Department, Lawrence Berkeley National Laboratory, Berkeley, CA, USA, [12]Department of Biology, Indiana University, Bloomington, IN, USA

Abstract Most Earth system models (ESMs) do not explicitly represent the carbon (C) costs of plant nutrient acquisition, which leads to uncertainty in predictions of the current and future constraints to the land C sink. We integrate a plant productivity-optimizing nitrogen (N) and phosphorus (P) acquisition model (fixation & uptake of nutrients, FUN) into the energy exascale Earth system (E3SM) land model (ELM). Global plant N and P uptake are dynamically simulated by ELM-FUN based on the C costs of nutrient acquisition from mycorrhizae, direct root uptake, retranslocation from senescing leaves, and biological N fixation. We benchmarked ELM-FUN with three classes of products: ILAMB, a remotely sensed nutrient limitation product, and CMIP6 models; we found significant improvements in C cycle variables, although the lack of more observed nutrient data prevents a comprehensive level of benchmarking. Overall, we found N and P co-limitation for 80% of land area, with the remaining 20% being either predominantly N or P limited. Globally, the new model predicts that plants invested 4.1 Pg C yr^{-1} to acquire 841.8 Tg N yr^{-1} and 48.1 Tg P yr^{-1} (1994–2005), leading to significant downregulation of global net primary production (NPP). Global NPP is reduced by 20% with C costs of N and 50% with C costs of NP. Modeled and observed nutrient limitation agreement increases when N and P are considered together (r^2 from 0.73 to 0.83).

Plain Language Summary Climate models do not take into account the carbon (C) spent by plants to acquire nutrients, such as nitrogen (N) and phosphorus (P). This can lead to uncertainties in future climate predictions. In this study, we integrate a model of plant nutrient acquisition using optimization methods (fixation & uptake of nutrients, FUN) into the energy exascale Earth system land model (ELM). Global plant N and P uptake are dynamically simulated by ELM-FUN based on the C costs of nutrient acquisition from multiple acquisition pathways. We benchmarked ELM-FUN with measurements (in situ, remotely sensed, and integrated using artificial intelligence), and other climate CMIP6 models. We found improvements in the global C cycle. Overall, we found N and P co-limitation for 80% of the land. Globally, the new model predicts that plant productivity is reduced by 20% with C costs of N and 50% with C costs of NP.

Key Points:

- We integrate a plant productivity-optimizing nitrogen and phosphorus acquisition model into the Energy Exascale Earth System Land Model
- We benchmarked the new model and found significant improvements in the carbon cycle. Nitrogen and phosphorus co-limit 80% of the land area
- Global Net Primary Production is reduced by 50% when the cost of nitrogen and phosphorus acquisitions are considered at the same time

Supporting Information:

Supporting Information may be found in the online version of this article.

Correspondence to:

R. K. Braghiere,
renato.k.braghiere@jpl.nasa.gov

Citation:

Braghiere, R. K., Fisher, J. B., Allen, K., Brzostek, E., Shi, M., Yang, X., et al. (2022). Modeling global carbon costs of plant nitrogen and phosphorus acquisition. *Journal of Advances in Modeling Earth Systems*, *14*, e2022MS003204. https://doi.org/10.1029/2022MS003204

Received 18 MAY 2022
Accepted 6 AUG 2022

Author Contributions:

Conceptualization: R. K. Braghiere, J. B. Fisher, X. Yang, R. A. Fisher
Data curation: R. K. Braghiere
Formal analysis: R. K. Braghiere
Funding acquisition: J. B. Fisher, X. Yang
Investigation: R. K. Braghiere
Methodology: R. K. Braghiere, J. B. Fisher, K. Allen, E. Brzostek, M. Shi,

1. Introduction

Terrestrial ecosystems have been a persistent post-industrial carbon (C) sink, absorbing almost a third of all anthropogenic C emissions (Arora et al., 2020; Ciais et al., 2013; Friedlingstein et al., 2019; Schimel et al., 2015). It remains uncertain whether this rate of uptake will persist in the future (Friedlingstein et al., 2006, 2014; Zhang et al., 2019), although it is broadly expected that limiting factors such as nutrient availability might mediate the responses of terrestrial ecosystems to elevated CO_2 and climate change (Fleischer et al., 2019; Terrer et al., 2019; Wieder et al., 2015a, 2019; Zaehle et al., 2010). Earth system models (ESMs) allow comprehensive and spatially explicit assessment of the impacts of environmental changes on biogeochemical cycles in terrestrial ecosystems.

X. Yang, D. M. Ricciuto, R. A. Fisher, R. P. Phillips
Project Administration: J. B. Fisher
Resources: R. K. Braghiere, J. B. Fisher, X. Yang, D. M. Ricciuto, R. P. Phillips
Software: R. K. Braghiere, J. B. Fisher, K. Allen, E. Brzostek, M. Shi, X. Yang, D. M. Ricciuto, R. A. Fisher
Validation: R. K. Braghiere
Visualization: R. K. Braghiere
Writing – original draft: R. K. Braghiere
Writing – review & editing: R. K. Braghiere, J. B. Fisher, K. Allen, E. Brzostek, M. Shi, X. Yang, D. M. Ricciuto, R. A. Fisher, Q. Zhu, R. P. Phillips

The natural sources and rates of supply of nitrogen (N) and phosphorus (P) are substantially distinct. While N availability is essentially unlimited as an atmospheric gas (N_2), although highly reliant on fixers, P comes from rock phosphate, renewed with the uplift of continental rock in geological timescales (Guignard et al., 2017). Apart from these significant differences in availability and turnover time, both nutrients play a crucial role on photosynthetic processes, cell growth, metabolism, and protein synthesis, while nucleic acids are approximately made of 39% N and nearly 9% P by mass (Chapin et al., 2000; Guignard et al., 2017; Sterner & Elser, 2002). Understanding how these nutrients limit plant productivity has been largely explored through observations (Chapin et al., 1986; Du et al., 2020; Fay et al., 2015; Hou et al., 2020; LeBauer & Treseder, 2008; Vitousek & Howarth, 1991), but global spatial patterns of terrestrial N and P limitation still remain a fundamental question for the fields of terrestrial ecology and biogeochemistry.

Some ESMs or their land components, the land surface models (LSMs), now include some representation of the N and P cycles, reflecting the relevance of nutrients as an important limiting factor across much of the Earth's land C assimilation (Fleischer et al., 2019; LeBauer & Treseder, 2008; Terrer et al., 2019). In the latest coupled model intercomparison project phase 6 (CMIP6; Eyring et al. (2016)), at least 10 ESMs considered N cycling (Arora et al., 2020; Jones et al., 2016), although only one—ACCESS/CABLE (Kowalczyk et al., 2013; Wang et al., 2011)–included P dynamics (Goll et al., 2012; Thum et al., 2019; Wang et al., 2007; Yang et al., 2019; Zhu et al., 2019). Arora et al. (2020) suggested that model uncertainty is reduced in the CMIP6 simulations when N cycling is included. However, most of these models assume that N and P are unrealistically acquired at no C cost to plants (Davies-Barnard et al., 2020), or these costs are to an extent implicitly included in autotrophic respiration, but without explicitly representations. This cost is often thought of as C assimilates that would otherwise be allocated as C to plant growth, that is, net primary production (NPP). In fact, omitting the C costs of N and P acquisitions may have significant impacts on the total C uptake estimates, as well as on the size and dynamic of N and P predicted by ESMs (Fisher et al., 2010; Ostle et al., 2009; Shi et al., 2016).

Autotrophic respiration is generally treated in LSMs as maintenance and growth respiration fluxes separately. Maintenance respiration is defined as the C cost to support the metabolic activity of plant living tissues, while growth respiration is defined as the additional C cost for the synthesis of new growth (Oleson et al., 2013). While maintenance respiration is associated with protein and membrane turnover and maintenance of ion concentrations and gradients, growth respiration is associated with growth processes such as synthesis of new structures in growth (Lötscher et al., 2004). Note that neither maintenance, nor growth respiration terms explicitly account for the C costs of nutrient acquisition. The most common pathways in which a plant expends energy or C costs for nutrient acquisition are resorbing (or retranslocating, these terms are used interchangeably) nutrients from senescing leaves, mobilizing and taking up nutrients that are locked in mineral soils or organic matter, maintain symbioses in the rhizosphere (mycorrhizae) through C exudates (Hobbie, 2006; Hobbie & Hobbie, 2008; Högberg & Högberg, 2002; Parniske, 2008), and biological N fixation (Dickinson et al., 2002; Guignard et al., 2017; Rastetter et al., 2001; Shi et al., 2016; Vitousek et al., 2002; Vitousek & Field, 1999; Wang et al., 2007). While it is well-known that plants allocate a part of the available C to acquire N and P from multiple acquisition pathways, only a few studies have attempted to quantify the variable C costs of N and P acquisition at the same time from each uptake pathway separately (Allen et al., 2020; Brzostek et al., 2014; Fisher et al., 2010; Shi et al., 2016).

Some evidence suggests that trees can allocate up to 20% of NPP to symbiotic and free-living microbes in the rhizosphere to increase their access to N (Brzostek et al., 2015; Hobbie, 2006; Högberg & Högberg, 2002). By accounting for N and P limitation at the same time, some ESMs project reductions in global NPP by as much as 25% (Allen et al., 2020; Goll et al., 2012; Wang et al., 2010), with some models suggesting that the land surface will become a source of C to the atmosphere by the end of the 21st century (Wieder et al., 2015a), although still highly debatable (Brovkin & Goll, 2015; Sun et al., 2017; Wieder et al., 2015b).

To represent C costs of N acquisition in ESMs, Fisher et al. (2010) introduced the fixation and uptake of nitrogen (FUN1.0) model, which is based on an optimal allocation theory whereby plants optimize the allocation of C used to acquire nutrients from the soil (directly through roots or from mycorrhizal associations), senescing leaves, and symbiotic biological N fixation to maximize growth (Bloom et al., 1985; Rastetter et al., 1997). Brzostek et al. (2014) integrated C–N trade-offs of arbuscular mycorrhizae (AM) and ectomycorrhizae (ECM) fungi into FUN (FUN2.0), which significantly improved dynamic predictions of N retranslocated from leaves and taken up from the soil. Afterward, Shi et al. (2016) coupled FUN2.0 into the Community Land Model version 4.0 (CLM4) (Bonan et al., 2011; Koven et al., 2013; Oleson et al., 2010) and Cai et al. (2016) coupled FUN into Noah-MP

(Niu et al., 2011). FUN2.0 was then further developed and carried into CLM5 (Fisher et al., 2019; Lawrence et al., 2019; Wieder et al., 2019).

The incorporation of P dynamics into FUN2.0, mirroring the existing model structure for N, led to a new model version, FUN3.0 (with a name update: FUN, Allen et al., 2020). Here, we couple FUN3.0 into the energy exascale Earth system model (E3SM) land model (ELM; Caldwell et al., 2019; Golaz et al., 2019; Yang et al., 2019; Burrows et al., 2020) to explore the sensitivity of the land surface C uptake to a dynamic C cost of N and P acquisition at the same time at global level. We evaluate variability across plant functional types (PFTs) to understand which ecosystems are the most N and P limited. We investigate how the C costs of N and P acquisition vary spatially, and determine how sensitive the land C sink is to a dynamic prediction of the C costs of N and P acquisition.

2. Materials and Methods

2.1. The Fixation and Uptake of Nutrients (FUN) Model (FUN3.0)

Within FUN, plants use C for N or P uptake by preferentially using dynamically varying pathways that are "cheaper" to them. Decreasing nutrient availability in soil and leaves leads to higher C expenditure on nutrient uptake and thus reduced growth (Fisher et al., 2019). In the original FUN1.0 model, plants obtain N through the following alternative and most common pathways: (a) active uptake, (b) retranslocation, and (c) symbiotic biological N fixation, which presents concurrent costs in terms of C, determined by the abundance of N in soils and plant tissues, and the temperature-dependent cost of N fixation (Bloom et al., 1985; Fisher et al., 2019; Jiang et al., 2017; Rastetter et al., 2001; Riahi et al., 2017; Terrer et al., 2018). The full model description and further analysis can be found in previous publications (Allen et al., 2020; Brzostek et al., 2014; Fisher et al., 2010; Shi et al., 2016). The full set of model equations can be found in Text S1 in Supporting Information S1.

Following the same approach as the original FUN1.0 model, FUN2.0 includes differential costs of active N uptake between ECM, AM, and non-mycorrhizal plants building upon the simultaneous N uptake from different pathways such as resistors in parallel using the Ohm's law (Brzostek et al., 2014). Allen et al. (2020) integrated P dynamics into FUN2.0 by incorporating the direct C cost of P uptake on top of the C cost of N uptake into a new model formulation, that is, FUN3.0. FUN3.0 was validated over 45 temperate forest plots in Indiana, USA, and 18 tropical dry forest plots in Guanacaste, Costa Rica. The validation sites varied in P availability and mycorrhizal associated tree types. FUN3.0 provides an important framework for predicting coupled N and P limitation within ESMs to enhance predictions of ecosystem response to global change.

The optimal allocation framework of FUN2.0 has been coupled into CLM4.5 and CLM5 (Brzostek et al., 2014; Fisher et al., 2019; Lawrence et al., 2019; Shi et al., 2016, 2019). Here, we take a similar approach to integrating the P dynamics of FUN3.0 into the E3SM land model (ELM: Ricciuto et al., 2018; Riley et al., 2018; Holm et al., 2020). ELM-FUN is based on the Converging Trophic Cascade (CTC) biogeochemistry framework, which includes P dynamics (Yang et al., 2016) and plant storage pools as new capabilities.

Root biomass impacts nutrient root uptake as described in Equation S3 in Supporting Information S1 and nutrient allocation distributed among different plant organs follows Metcalfe et al. (2017). For a complete description of the CNP cycles in ELM, including plant allocation and other fluxes please refer to Burrows et al. (2020).

Features in ELM include: (a) prognostic P cycle and C-N-P interactions; (b) mortality rates for tropical forests based on soil physical factors (Galbraith et al., 2013); and (c) C, N, and P non-structural vegetation storage pools. The P pools and fluxes are based on a previous modeling study that implemented the P cycle into CLM4 (Yang, Thornton, et al., 2014). The P cycle is vertically resolved, capturing the dynamics of inorganic P pools, the conversion between organic P and inorganic P in each soil layer, as well as the vertical transport of P pools between layers (Yang et al., 2019). Allocation to structural plant pools is calculated using available C and available non-structural nutrients after the remaining C (assimilation minus maintenance respiration) is allocated to a non-structural C storage pool following Metcalfe et al. (2017). Flexible plant tissue stoichiometry is not considered in the model.

Vegetation is divided into multiple PFTs with independent parameterizations controlling photosynthesis, leaf gas exchange, biomass allocation, and other processes (Sulman et al., 2021). The current PFT configuration of ELM

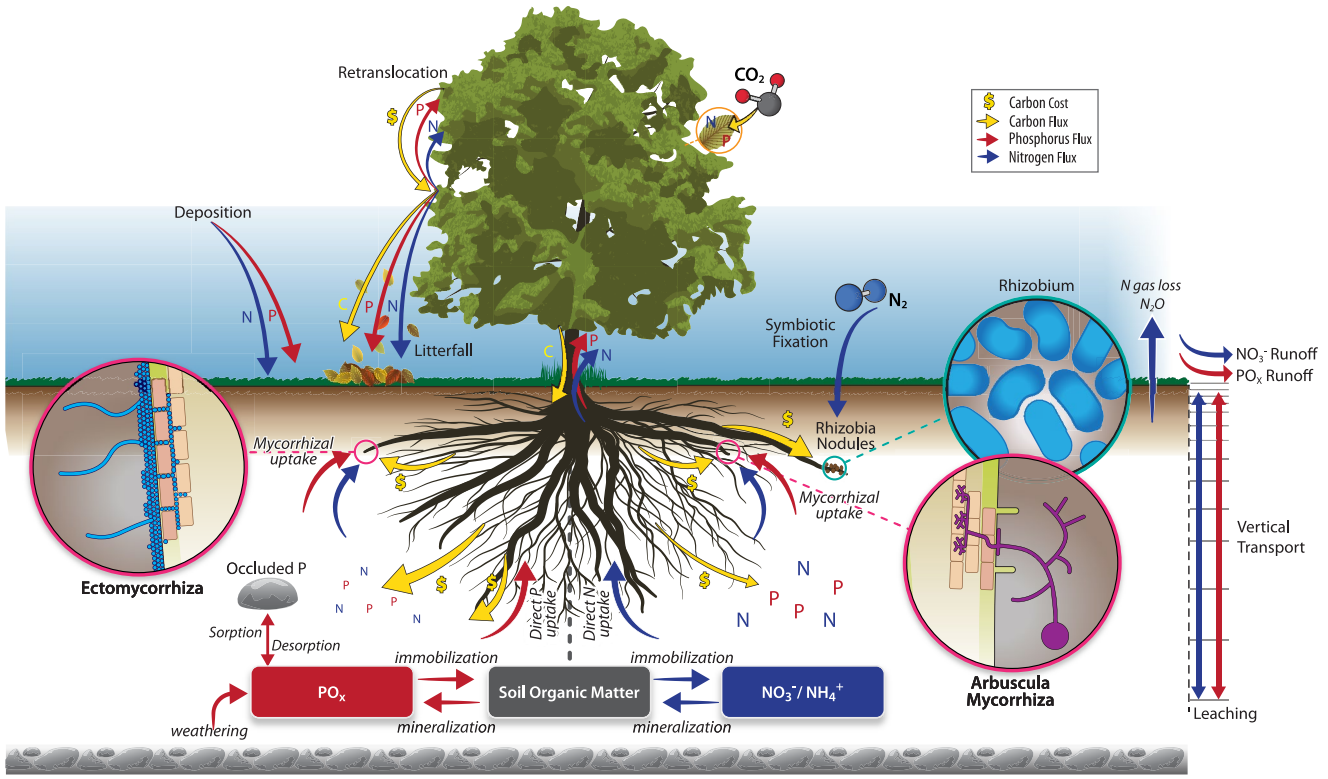

Figure 1. Illustration of Energy Exascale Earth System Model (E3SM) Land Model (ELM)–fixation and uptake of nutrients (ELM-FUN) major features including C costs of NH_4^+, NO_3^-, and PO_x uptake through multiple pathways including: (a) leaf nutrient retranslocation (resorption); (b) differentiation between two types of mycorrhizal fungi (ECM vs. AM); (c) direct root uptake; and (d) free-living N_2 biological fixation.

follows CLM5; Lawrence et al. (2019), which are based on broad plant groups relevant for global-scale configurations (Wullschleger et al., 2014).

To generate the trade-offs between AM, ECM, and non-mycorrhizal root uptake, FUN3.0 needs an estimate of the percentage of aboveground biomass that associates with each mycorrhizal type for each model grid cell (Braghiere, Fisher, et al., 2021; Brzostek et al., 2014; Shi et al., 2016). Each PFT was classified based on commonly known associations between the specific plant species and either AM- and ECM-fungi. As a result, some PFTs are largely AM-dominated (e.g., grasslands, crops) and some are ECM-dominated (e.g., boreal forest) (Allen et al., 1995; Phillips et al., 2013; Read, 1991).

These PFT fractions are coarse and do not extensively capture the spatial heterogeneity in mycorrhizal association, particularly in mixed-mycorrhizal PFTs, such as tropical (Waring et al., 2016) and temperate forests (Phillips et al., 2013). However, recent comparisons with a global map of mycorrhizal association (Steidinger et al., 2019) indicate the robustness of this assumption (Braghiere, Fisher, et al., 2021). Regarding N fixation, following the implementation in CLM5 (Fisher et al., 2019) each PFT has an associated maximum fraction of the C acquisition that can be used for fixing N, defined as a constant fraction for natural PFTs (25%). The fractions of the AM- and ECM-associated plants in association with ELM PFTs are shown in Table S3 in Supporting Information S1. The spatial patterns in nutrient uptake pathways are driven by a combination of the PFT distribution plus any other non-PFT spatial information that impacts the FUN model. In LSMs, a vegetated unit with multiple PFTs is associated with a single soil column. FUN3.0 was coupled to ELM using thirteen input variables (Table S1 in Supporting Information S1) with most of them being directly calculated by the C-N-P processes of ELM including: available soil N (N_{soil}) and available soil P (P_{soil}), fine root biomass (C_{root}), leaf N before senescence (N_{leaf}), leaf P before senescence (P_{leaf}), NPP (C_{NPP}), soil temperature (T_{soil}), and evapotranspiration (ET). The derivation and direct usage of variables from ELM to generate the necessary inputs for FUN3.0, as well as the key modifications needed to enable the coupling between FUN3.0 and ELM can be found in Supporting Information S1. A diagram of the coupled model is shown in Figure 1.

2.2. Model Configuration and Simulations

Global simulations were performed at hourly 1.9° × 2.5° spatiotemporal resolution. All three model simulations were spun up using ELM for 200 years of accelerated decomposition mode, followed by 600 years of regular spin up (Koven et al., 2013; Thornton & Rosenbloom, 2005), while soil P pools were initialized from observations (Yang et al., 2013) at the beginning of the regular spin up. Some processes governing the global distribution of soil P stocks operate in geologic time scales, which makes it impossible at this time to perform a fully prognostic model spin up from "bare ground" conditions to initialize P pools with slow turnover times. Instead, ELM relies on global maps of soil phosphorus pools synthesized from observations (Yang & Post, 2011; Yang, Post, et al., 2014), which have previously been used successfully in land model simulations using prescribed atmospheric forcings (Burrows et al., 2020; Yang et al., 2016). Spin up was followed by historical transient simulations (1850–2010) with historical atmospheric CO_2, N deposition (Lamarque et al., 2005), P deposition (Mahowald et al., 2005), land use change (Hurtt, 2018), and using the Global Soil Wetness Project 3 (GSWP3) climate forcing (Dirmeyer et al., 2006). We analyzed a 12 year (1994–2005) period and investigated the role of N and P in affecting the responses of NPP to three configurations of the model: ELM only (CNP cycles without the FUN model), ELM-FUN2.0 (CNP cycles with the FUN model for N only), and ELM-FUN3.0 (CNP cycles with the FUN model for N and P). These factorial experiments allow us to disentangle the impacts of N and P in isolation and in combination.

2.3. Model Benchmarking

We use the International Land Model Benchmarking (ILAMB) v2.6 package for model validation (Collier et al., 2018) focusing on global patterns of the C and water cycle variables, including datasets of: (a) aboveground living biomass based on inventory plots upscaled to the globe using remote sensing imagery (Saatchi et al., 2011); (b) emulated CO_2 concentrations from the NOAA/ESRL flask network (http://www.esrl.noaa.gov/gmd/ccgg/); (c) FLUXCOM GPP and ecosystem respiration (Jung et al., 2019, 2020); (d) leaf area index (LAI) from the Moderate Resolution Imaging Spectroradiometer (MODIS) (de Kauwe et al., 2011); (e) global net ecosystem C balance from the Global Carbon Project (Le Quéré et al., 2016) and Hoffman et al. (2014); (f) net ecosystem exchange (NEE) from FLUXNET2015 (Pastorello et al., 2020); (g) the top 1-m soil C stock with the Harmonized World Soil Database (HWSD; Todd-Brown et al., 2013); and (viii) evapotranspiration (ET) from the Global Land Evaporation Amsterdam Model (GLEAM) v3.3a (Martens et al., 2017).

The relationships of the evaluated variables with precipitation, temperature, and surface incident shortwave radiation were performed using data products from the global precipitation climatology project (GPCP) Monthly Analysis version 2.3 (Adler et al., 2018), the climatic research unit (CRU) monthly temperature version 4.02 (Harris et al., 2014), and the clouds and the earth's radiant energy system (CERES) surface irradiances edition 4.1 (Kato et al., 2018; Loeb et al., 2018).

We show the results for the ILAMB overall score for the absolute values (S_{overall}), as well as their relationships with precipitation, incident shortwave radiation, and temperature ($S_{\text{overall}}^{\text{relationship}}$) defined as:

$$S_{\text{overall}} = \frac{S_{\text{bias}} + 2S_{\text{RMSE}} + S_{\text{phase}} + S_{\text{iav}} + S_{\text{dist}}}{1 + 2 + 1 + 1 + 1} \tag{1.1}$$

$$S_{\text{overall}}^{\text{relationship}} = \frac{S_{\text{RMSE}}^{P} + S_{\text{RMSE}}^{\text{SW}} + S_{\text{RMSE}}^{T}}{1 + 1 + 1} \tag{1.2}$$

where S_{bias} is the spatially integrated bias score, S_{RMSE} is the root-mean-squared error (RMSE) score doubly weighted to emphasize its importance, S_{phase} is the phase shift score, S_{iav} is the interannual variability score, and S_{dist} is the spatial distribution score in Equation 1.1. $S_{\text{RMSE}}^{\text{x}}$ is the spatial RMSE score for each x meteorological variable in Equation 1.2. For the whole set of equations of each term in Equations 1.1 and 1.2, and further details refer to Collier et al. (2018).

NPP results from our simulations are also compared with the NPP from 11 CMIP6 models (the same 11 models evaluated in Arora et al. (2020)), MODIS (Running & Zhao, 2015; Running et al., 2004; Zhao et al., 2005), and the International Satellite Land-Surface Climatology Project, Initiative II (ISLSCP II) collection from the International Geosphere Biosphere Program (IGBP) (Cramer et al., 1999). Projects such as the CMIP6 (Eyring

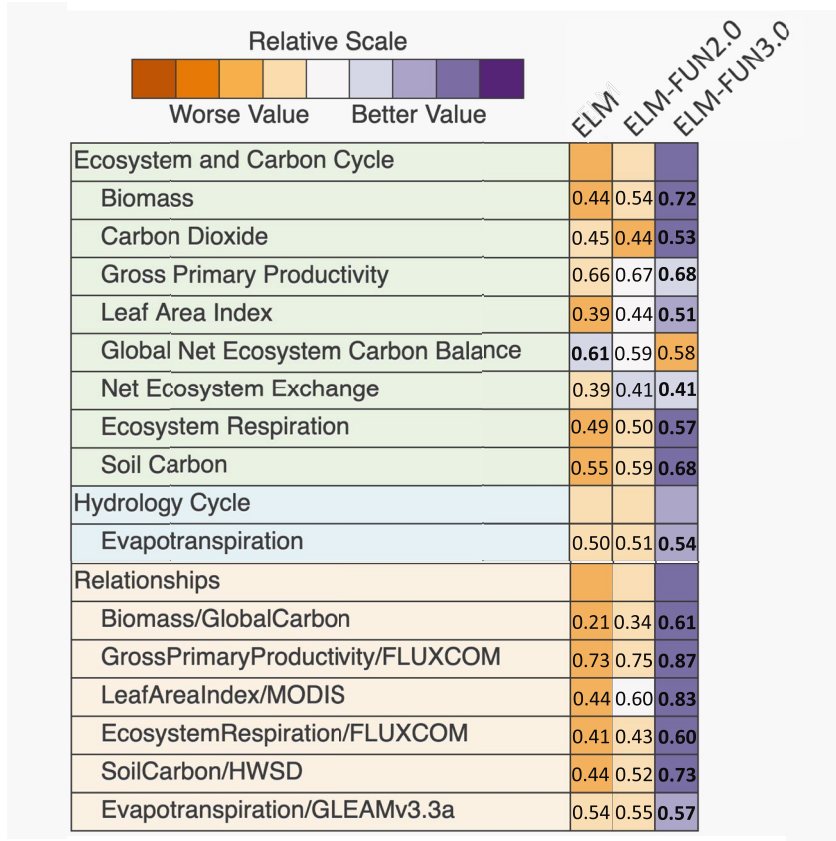

	ELM	ELM-FUN2.0	ELM-FUN3.0
Ecosystem and Carbon Cycle			
Biomass	0.44	0.54	**0.72**
Carbon Dioxide	0.45	0.44	**0.53**
Gross Primary Productivity	0.66	0.67	**0.68**
Leaf Area Index	0.39	0.44	**0.51**
Global Net Ecosystem Carbon Balance	**0.61**	0.59	0.58
Net Ecosystem Exchange	0.39	0.41	**0.41**
Ecosystem Respiration	0.49	0.50	**0.57**
Soil Carbon	0.55	0.59	**0.68**
Hydrology Cycle			
Evapotranspiration	0.50	0.51	**0.54**
Relationships			
Biomass/GlobalCarbon	0.21	0.34	**0.61**
GrossPrimaryProductivity/FLUXCOM	0.73	0.75	**0.87**
LeafAreaIndex/MODIS	0.44	0.60	**0.83**
EcosystemRespiration/FLUXCOM	0.41	0.43	**0.60**
SoilCarbon/HWSD	0.44	0.52	**0.73**
Evapotranspiration/GLEAMv3.3a	0.54	0.55	**0.57**

Figure 2. ILAMB C cycle, ET, and their relationships with precipitation, incident shortwave radiation, and temperature summary scores for Earth land model (ELM), ELM-fixation & uptake of nutrients2.0 (ELM-FUN2.0), and ELM-FUN3.0. Shown are the overall scores for various variables and the colors represent relative scores. Values in bold represent the best overall scores.

et al., 2016) have allowed for consistent comparison of the response of the C cycle under climate change from existing state-of-the-art ESMs. Using CMIP6 outputs together with satellite observations allow us to estimate the range uncertainty in C cycle variables due to model structural variation. We note that our simulations are done offline with atmospheric forcing data, such as in LUMIP (Lawrence et al., 2016) and TRENDY (Sitch et al., 2015), while CMIP models also simulate atmospheric states in coupled runs through the historical period.

In addition, we compared estimates of biological N fixation with a recent compilation of 12 studies by Davies-Barnard and Friedlingstein (2020), plus estimates by Sullivan et al. (2014) and Peng et al. (2020). We also added an explicit comparison with predicted N and P limitation values presented in Du et al. (2020) and generated an agreement map between both data products.

3. Results

3.1. Benchmarking ELM-FUN

Coupling both recent versions of FUN into ELM improved the overall normalized standard deviation between model and observation for all the evaluated variables in ILAMB (Figure 2). Moreover, FUN3.0 improves model performance even further when compared to FUN2.0. Although most of the evaluated variables were improved to some degree, the largest improvements were found for biomass (Figure S1a in Supporting Information S1), LAI (Figure S1d in Supporting Information S1), and soil C (Figure S1f in Supporting Information S1).

The relationships of the evaluated variables with precipitation, incident shortwave radiation, and temperature also improved with ELM-FUN3.0 (Figure 2). All the ILAMB plots comparing ELM, ELM-FUN2.0, and ELM-FUN3.0 are available from https://braghiere.github.io/ILAMB_ELM_FUN_reduced_v1/.

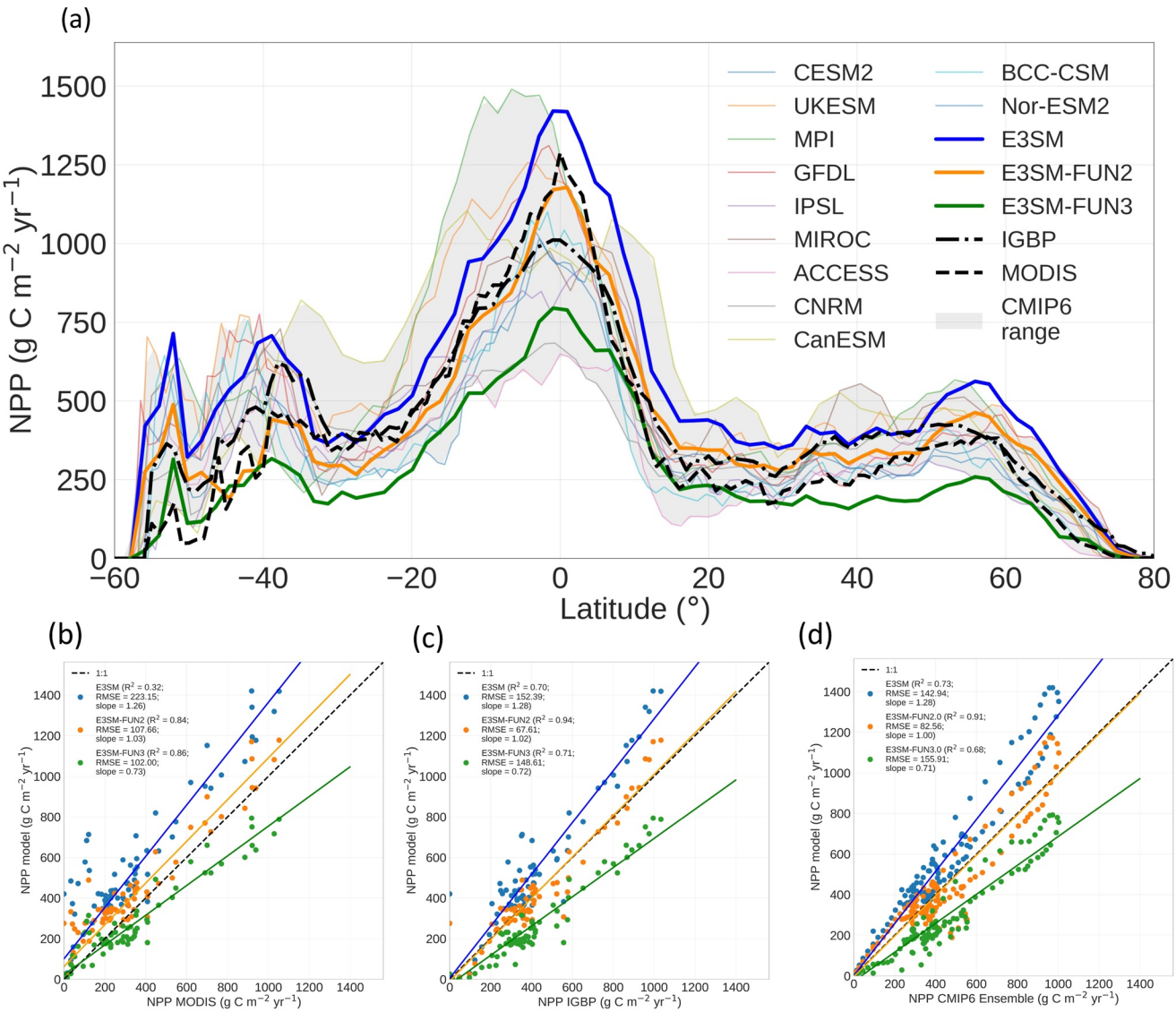

Figure 3. (a) The annual (1994–2005) zonal mean net primary production (NPP) (g C m^{-2} yr^{-1}) simulated by ELM, ELM-FUN2.0 (FUN2, C costs of N only), ELM-FUN3.0 (FUN3, C costs of N and P together), the zonal mean NPP from the 11-member ensemble of CMIP6 models, MODIS NPP, and IGBP NPP; (b) scatter plot between zonal mean annual NPP from three configurations of ELM (default, FUN2, and FUN3) and MODIS NPP, IGBP NPP, and NPP from the ensemble member of 11 CMIP6 models. The r^2, RMSE, and slope values are shown in brackets.

ELM-FUN2.0 simulates mean NPP of 51.2 Pg C yr^{-1} (1994–2005), which is 13.6 Pg C yr^{-1} less than that simulated by ELM for the same period. This implies a downregulation of global annual NPP by 21.0%. Zonally, NPP was reduced across all latitudes in ELM-FUN2.0 relative to ELM (Figure 3a). In ELM-FUN3.0, NPP was 32.2 PgCyr^{-1} on average from 1994 to 2005, which is 32.6 PgCyr^{-1} less than that simulated by ELM for the same period, a reduction of 50.3% in global annual NPP. Zonally, NPP was reduced across all latitudes in ELM-FUN3.0 relative to ELM (Figure 3). The drops in global NPP are larger than the direct costs of nutrient uptake due to feedbacks on LAI and GPP in the model. Additionally, the global mean C Use Efficiency (CUE; defined as NPP/GPP) is negatively impacted when considering the C costs of N and P acquisition (Figure S11b in Supporting Information S1), going from ~30% in ELM to ~20% in ELM-FUN3.0. Although CUE is a highly uncertain metric, previous studies indicate that natural ecosystems present a CUE of 32%–47% (Campioli et al., 2015; Malhi et al., 2009).

The NPP zonal mean (along the latitudinal component) from all three simulations with ELM are shown in scatter plots compared to the zonal mean of MODIS NPP (Figure 3b), IGBP NPP (Figure 3c), and the zonal mean NPP

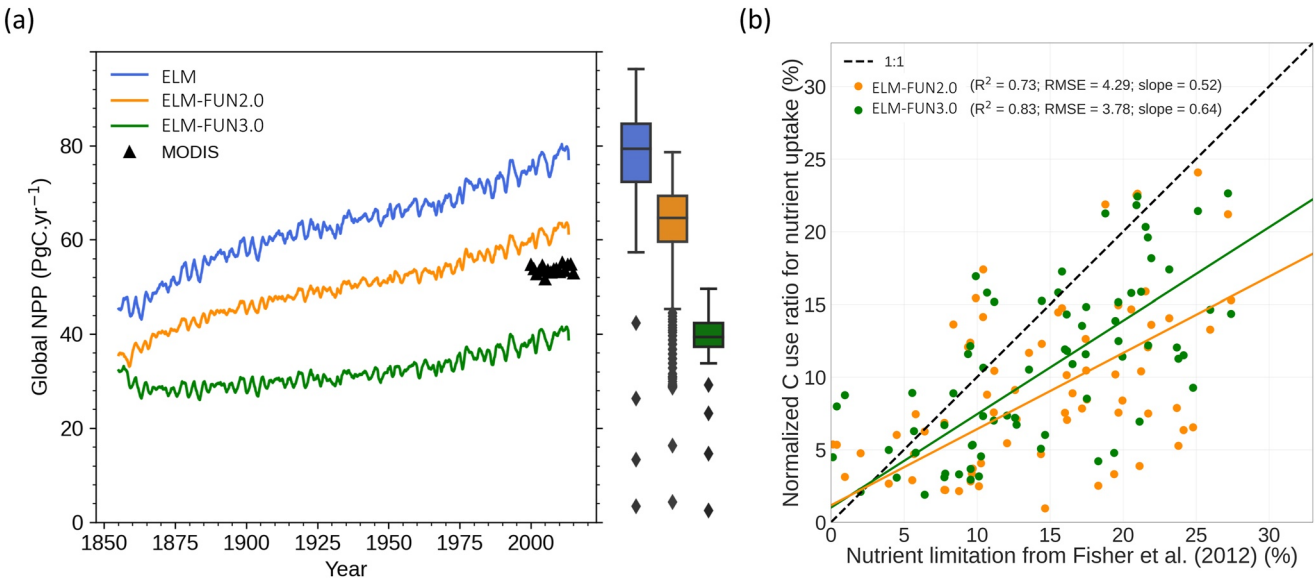

Figure 4. (a) Global net primary production (NPP) (PgC.yr^{-1}) over the historical period (1855–2010) for Earth land model (ELM), ELM-FUN2.0, and ELM-FUN3.0. Global MODIS NPP is also shown for reference (2000–2015). The box plot on the right-hand side indicates the NPP distribution for the historical period. Dots represent outliers not included in the box plot; (b) scatter plot of the mean (1994–2005) zonal normalized C use ratio for nutrient uptake (%) from ELM-FUN2.0 (N only), ELM-FUN3.0 (N and P together) versus the remotely sensed Total Nutrient Limitation product from Fisher et al. (2012). The 1:1 line is represented by the dashed black line. The r^2, RMSE, and slope values are show in brackets.

from the ensemble member of 11 CMIP6 models (Figure 3d). The implementation of FUN into ELM improved the relationships between ELM and all three data products. For MODIS NPP, considering the C costs of N acquisition in ELM increased the r^2 of the linear relationship from 0.32 to 0.84 and reduced the root mean squared error (RMSE) by 52% from 223.2 gCm^{-2}yr^{-1} to 107.7 gCm^{-2}yr^{-1}, while the slope also changed from 1.26 to 1.03. Adding the C costs of P acquisition on top of the costs of N acquisition increased r^2 to 0.86 and reduced the RMSE by 54%–102.0 gCm^{-2}yr^{-1}, while the slope changed to 0.73.

For the IGBP NPP linear relationship, the RMSE decreased 56% from 152.4 gCm^{-2}yr^{-1} with ELM to 67.6 gCm^{-2}yr^{-1} with ELM-FUN2.0%, and 2% to 148.61 gCm^{-2}yr^{-1} with ELM-FUN3.0. For the CMIP6 ensemble member NPP, the RMSE decreased 42% from 142.9 gCm^{-2}yr^{-1} with ELM to 82.6 gCm^{-2}yr^{-1} with ELM-FUN2.0, but increased 9% (155.9 gCm^{-2}yr^{-1}) with ELM-FUN3.0. The r^2, RMSE, and slope of all model runs and products are shown in Figure 3. In general, the relationships between modeled zonal NPP with ELM and these three data products seem to be improved when the C costs of nutrient acquisition are considered (Figure 3b), although the addition of both nutrients seems to underestimate NPP, potentially because of implicit compensating mechanisms already present in the ELM NPP without FUN. Although FUN3.0 directly represents the C costs of N + P acquisition, that does not mean the remaining parts of ELM are improved as well. This study does not intend to improve all the processes represented in the model.

Figure 4a shows global NPP transient simulations for the historical period (1850–2010) for the three model configurations and MODIS NPP (2000–2015) for reference. Global NPP presents a reduction of ∼20% when considering the C costs of N acquisition and ∼50% when considering the C costs of N and P at the same time. The MODIS NPP data product values are at the lower end of the ELM-FUN2.0 distribution and at the upper end of the ELM-FUN3.0 distribution.

FUN is dynamically coupled to ELM in the historical runs, that is, 1850–2010. However, during spin up (200 years in accelerated decomposition mode + 600 years in normal mode), the CNP pools are brought to equilibrium without the FUN model, that is, ELM only for all three model configurations as described in Section 2.2. The standard spin-up protocol is used to achieve C, water, and energy equilibrium at the start of the simulation (Lawrence et al., 2019). The specifics of a spin up method often vary according to model type and objectives, but generally it involves either running a model repeatedly using a single period of forcing data, or running a model for many

years with historical forcing data and evaluating model outputs after a time window long enough to achievement of steady state of the variable of interest.

The year 1850 equilibrium conditions were calculated by integrating over a repeating 20-year period of an atmospheric reanalysis data set (i.e., years 1901–1920 from the forcing data sets) along with fixed atmospheric CO_2, N deposition, and P deposition. As with earlier versions of ELM, it is prohibitively expensive to run the full model for the period of time required to achieve a quasi-steady state. Thus, the spin-up procedure involves an "accelerated decomposition" methodology introduced in Koven et al. (2013) and Thornton and Rosenbloom (2005). During the accelerated decomposition phase, the decomposition of the slow C pools (e.g., the long turnover time soil C and coarse woody debris pools) are artificially increased to allow faster convergence on the equilibrium state (Lawrence et al., 2019). Due to the processes in FUN accessing soil P, which operates in geologic time scales, ELM-FUN coupling starts after model spin up. Therefore, it is expected that in the initial years of the transient simulation, simulations with ELM–FUN versions show a pulse in autotrophic respiration during the first years because of a new C source to autotrophic respiration from FUN, but over time respiration declines relative to ELM (Figure S10 in Supporting Information S1). This behavior is also described in Shi et al. (2016) when evaluating the impacts of FUN in CLM. Nevertheless, the evaluations performed in this study focus on the period 1994–2005, or 144 years after model equilibrium was reached in order to minimize the possible impacts of the model initialization from cold start (Meier et al., 2018; Shi et al., 2016).

Among the few global nutrient cycling products available for model benchmarking, Fisher et al. (2012) coupled remotely sensed estimates of NPP and ET to identify areas where light and water are not limiting factors on productivity. Overall, the NPP downregulation fraction simulated by ELM–FUN3.0 presents a similar global spatial distribution to that of the nutrient limitation product from Fisher et al. (2012) (see Figure S2 in Supporting Information S1). Figure 4b shows a scatterplot between the zonal mean of nutrient limitation product from Fisher et al. (2012) and the zonal mean of the normalized C use ratio for N acquisition in FUN2.0, and N + P acquisition in FUN3.0. The C use ratio is defined as the ratio of C spent on N acquisition (FUN2.0) or N + P acquisition (FUN3.0) to the total C available to the plant. The normalized C use ratio is the C use ratio divided by the maximum C use ratio. The agreement between the modeled nutrient limitation and the observation-based estimate from Fisher et al. (2012) increases when N and P are considered together. The r^2 increases from 0.73 to 0.83 and the RMSE decreases from 4.3% to 3.7%.

3.2. Spatial Patterns of N and P Acquisition Strategies

Globally, the amount of N uptake and the pathway of N acquisition varied as a function of ecosystem productivity, dominant mycorrhizal type, soil nutrient availability, and environmental conditions. ELM–FUN3.0 simulated the mean annual global total N uptake as 841.8 Tg N yr^{-1}.

Mycorrhizal uptake and direct root uptake follow the spatial distribution of the most productive areas of the globe, but with significantly different magnitudes (Figure 5). While the global total mycorrhizal root uptake is 659.9 Tg N yr^{-1}, mostly due to AM fungi associations (73.0% of the total mycorrhizal root uptake or 482.1 Tg N yr^{-1}), with the remaining 27.0% due to ECM fungi association (177.8 Tg N yr^{-1}) (Figure 5); the direct root uptake is 84.3 Tg N yr^{-1}. These results are due to the differences in the C cost of uptake by mycorrhizal roots compared to non-mycorrhizal roots as defined in Table S2 in Supporting Information S1 and Allen et al. (2020), the spatial distribution of available soil N (Figure S3 in Supporting Information S1), and the spatial distribution of mycorrhizal types. Spatial differences among distinct mycorrhizal types are given by the PFT distribution following Table S3 in Supporting Information S1. The extra-tropics have lower rates of N uptake in comparison to the tropics, with higher values associated with mycorrhizal uptake and retranslocation in boreal forests, and direct root uptake over the tundra ecosystems. Arid and semi-arid areas of the world present the lowest N uptake (Figure 5).

Total biological N fixation comprises 35.3 Tg N yr^{-1}, nearly an order of magnitude lower than the total of mycorrhizal and non-mycorrhizal root uptake. In the northern hemisphere, temperate forests have higher symbiotic N fixation values than other ecosystems (Figure 5). The highest rates of symbiotic N fixation are in the tropics. This estimate is near the lowest boundary of a global compilation study suggesting that biological N fixation is between 52 and 130 Tg N yr^{-1} (Davies-Barnard & Friedlingstein, 2020) (Figure S8 in Supporting Information S1). Other studies highlight the need for more field measurements of N fixation (Peng et al., 2020), and while our low N fixation estimate is likely due to the fact that all fixed N goes into the plant directly, rather than going

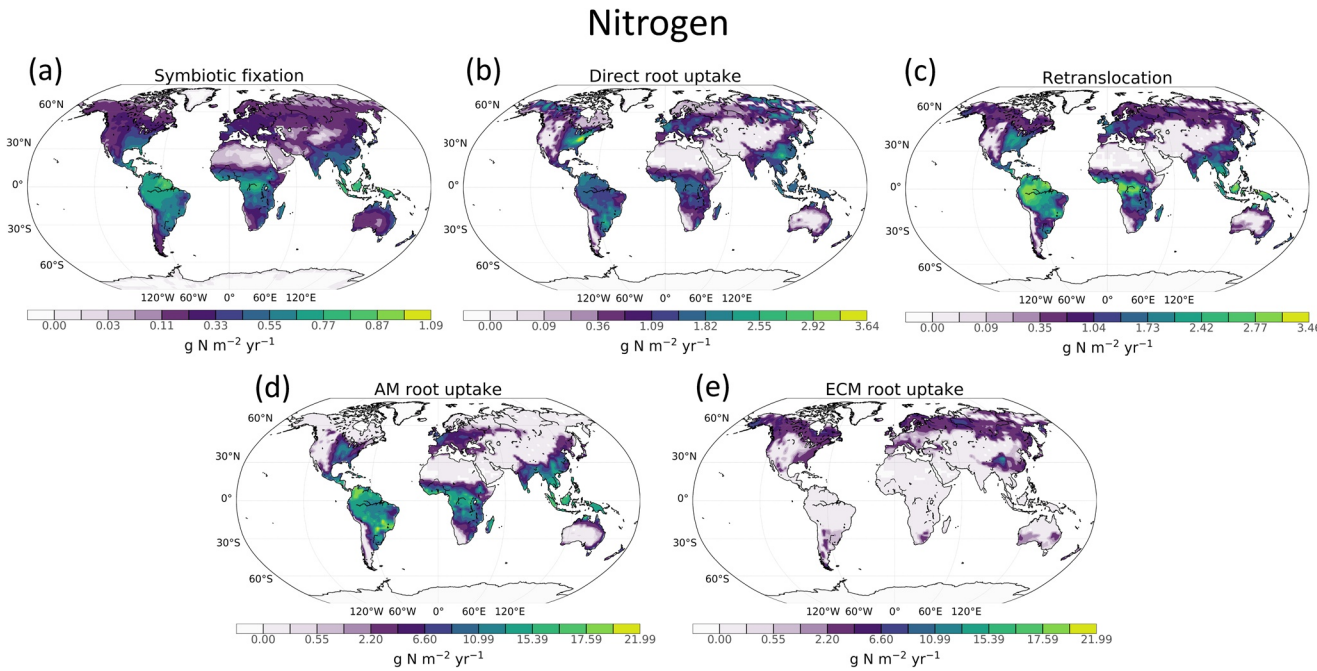

Figure 5. The global mean annual (1994–2005) (a) symbiotic biological N fixation, (b) direct root uptake (i.e., non-mycorrhizal root uptake; direct root uptake is called in the figures for short), (c) retranslocation, (d) arbuscular mycorrhizal (AM)-associated uptake, and (e) ectomycorrhizal (ECM)-associated N uptake (g N m^{-2} yr^{-1}) simulated by ELM-FUN3.0.

into soils first such as N from other active uptake pathways, a study presents evidence that N fixation may be lower than previously assumed (Sullivan et al., 2014).

The total amount of retranslocated N and P from leaves globally are 97.6 Tg N yr^{-1} and 7.3 Tg P yr^{-1}, respectively. Tropical and temperate forests, as well as grasslands and crop areas in the southeastern USA, Asia, and southern South America have relatively higher retranslocation rates (Figure 5). These high N and P retranslocation values are driven by high LAI and the proportional high leaf N and leaf P concentrations simulated by ELM-FUN3.0. Areas with low soil mineral N and low soil mineral P have high retranslocation rates and areas with low leaf N and low leaf P, such as the tundra and arid/semi-arid regions, have the lowest retranslocation rates (Figures 5c and 6b). Moreover, the retranslocation efficiency values for N and P, that is, the ratio of the retranslocated nutrient to the amount of nutrient in dead leaves prior to senescence, varies from less than 15% in grassland areas in China and southern South America, to up to 50% in the boreal regions for N and P, and savannas for N, which is in agreement with observations (Aerts, 1996). The tropics have a highly variable N retranslocation efficiency ranging from around 30% in the broadleaf evergreen forests to 50% over grasslands (Figure 7a), and a P retranslocation efficiency of around 40% (Figure 7b), which seems slightly underestimated in comparison to observational studies that indicate 50% (Aerts, 1996; Reed et al., 2012).

Similarly, both the rate of P uptake and the pathway of P acquisition varied as a function of ecosystem productivity and dominant mycorrhizal type globally. ELM–FUN3.0 simulated the mean annual global total P uptake of 48.1 Tg P yr^{-1}, compared to that simulated by E3SMv1.1-CTC of 42.0 Tg P yr^{-1} and by E3SMv1.1-ECA (Equilibrium Chemistry Approximation) of 63.0 Tg P yr^{-1} (Burrows et al., 2020). The spatial patterns in the global distribution of the three major P uptake pathways is shown in Figure 6. The mycorrhizal root uptake and the direct root uptake (i.e., the non-mycorrhizal root uptake) follow the spatial distribution of the most productive areas of the globe, but with significantly different magnitudes (Figure 6). The global total mycorrhizal root uptake is 20.0 Tg P yr^{-1}, due largely to AM, which is 55.4% of the total mycorrhizal root uptake (11.1 Tg P yr^{-1}) (Figure 6), with 44.6% of the remaining from ECM (8.9 Tg P yr^{-1}) (Figure 6); direct root uptake is 20.9 Tg P yr^{-1}. This is due to the differences in the C cost of uptake by mycorrhizal roots compared to non-mycorrhizal roots as defined in Allen et al. (2020) and the spatial distribution of soil available P (Yang, Thornton, et al., 2014,

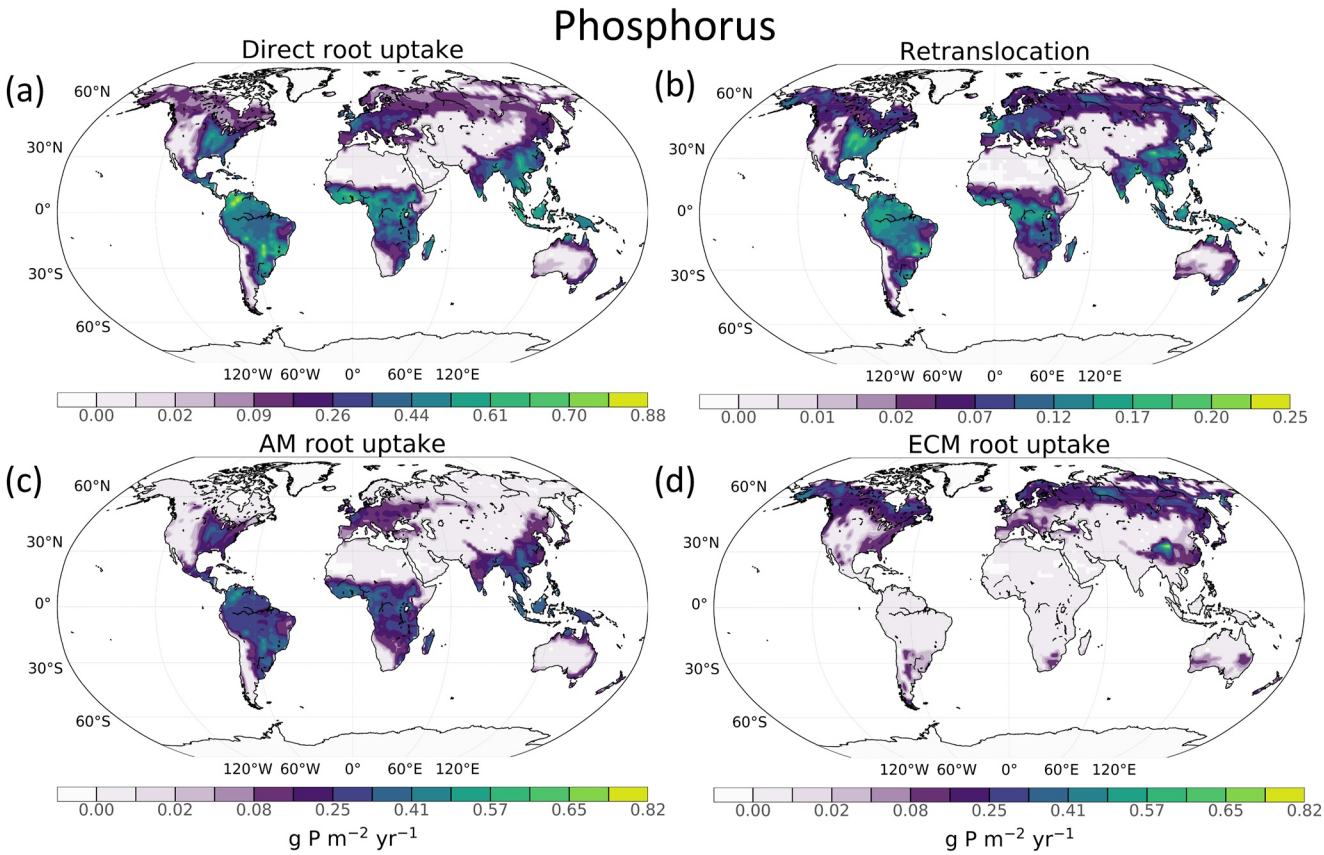

Figure 6. The global mean annual (1994–2005) (a) direct root uptake (i.e., non-mycorrhizal root uptake; direct root uptake is called in the figures for short), (b) retranslocation, (c) arbuscular mycorrhizal (AM)-associated uptake, and (d) ectomycorrhizal (ECM)-associated P uptake (g P m^{-2} yr^{-1}) simulated by ELM-FUN3.0.

Yang, Post, et al., 2014) (Figure S3 in Supporting Information S1). Most of the tropics, southeast South America, eastern USA, and southeast China have the largest values of soil N and P uptake globally. The boreal forests and tundra ecosystems have lower rates of P uptake in comparison to the tropics, with higher values associated with mycorrhizal uptake and retranslocation. Arid and semi-arid areas have the lowest P uptake (Figure 6).

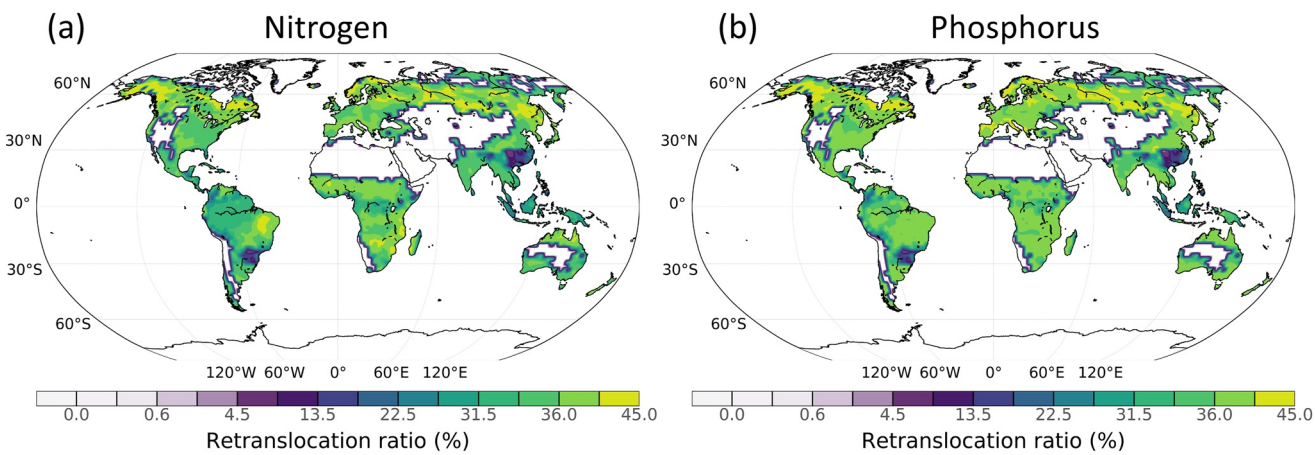

Figure 7. The global mean annual (1994–2005) retranslocation ratio of (a) N and (b) P simulated by Earth land model-fixation & uptake of nutrients3.0. The retranslocation ratio is defined as the retranslocated N or P to the amount of N or P in dead leaves prior to senescence.

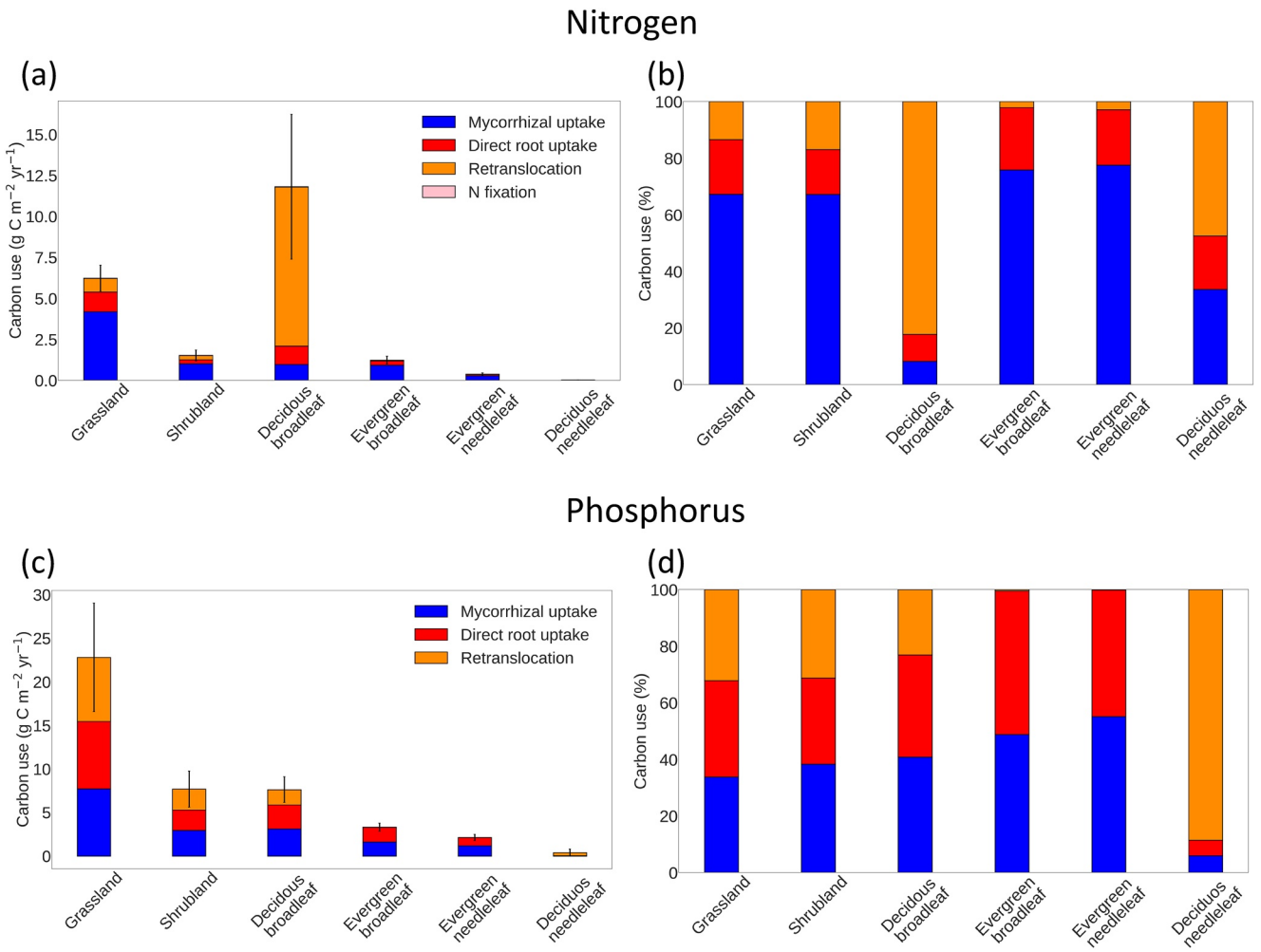

Figure 8. The global mean annual (1994–2005) C used by (a) N total acquisition and (b) relative acquisition, and; (c) P total acquisition and (d) relative acquisition in evergreen broadleaf forest, evergreen needleleaf forest, deciduous broadleaf forest, grassland, shrubland, and deciduous needleleaf forest. Error bars are ±1 standard deviation.

3.3. How Does the C Costs of N and P Acquisition Vary According to Different PFTs?

ELM-FUN3.0 estimated that 8% of NPP or 2.5 Pg C yr^{-1} was spent by plants to take up N. The two largest amounts of C were spent on mycorrhizal root uptake (i.e., 1891.7 Tg C yr^{-1} or 74.9%) and on direct root uptake (i.e., 623.0 Tg C yr^{-1} or 24.7%), respectively. The C spent on retranslocation was 20.6 Tg C yr^{-1}, which corresponds to 0.42% of the total used C. The C spent on N fixation was 0.8 Tg C yr^{-1}, which corresponds to 0.03% of the total used C.

ELM-FUN3.0 estimated that 5% of NPP or 1.6 Pg C yr^{-1} was spent by plants to acquire P. The two largest C expenditure fluxes were direct root uptake (i.e., 859.6 Tg C yr^{-1} or 52%) and mycorrhizal root uptake (i.e., 781.6 Tg C yr^{-1} or 47%), respectively. C spent on retranslocation was 4.2 Tg C yr^{-1}, which corresponds to 0.26% of the total used C.

Direct root uptake and mycorrhizal uptake were the two pathways where the majority of C expenditure was predicted. However, the expenditure of C is heavily dependent on PFT (Figure 8). Grasslands had the highest C use rate for P acquisition (22.8 ± 6.2 g C m^2 yr^{-1}) with 32% of the total C spent on P acquisition used to support retranslocation (Figure 8). Shrublands showed similar total C expenditure to deciduous broadleaf forests, with 38% and 40% of the total C spent on P acquisition used to support mycorrhizal root uptake, respectively. Evergreen broadleaf and evergreen needleleaf forests had a total C use rate of 3.3 ± 0.5 g C m^2 yr^{-1} and 2.1 ± 0.3 g C m^2 yr^{-1}, respectively. In terms of the main uptake pathway, mycorrhizae represent 49% and 55% of the total C

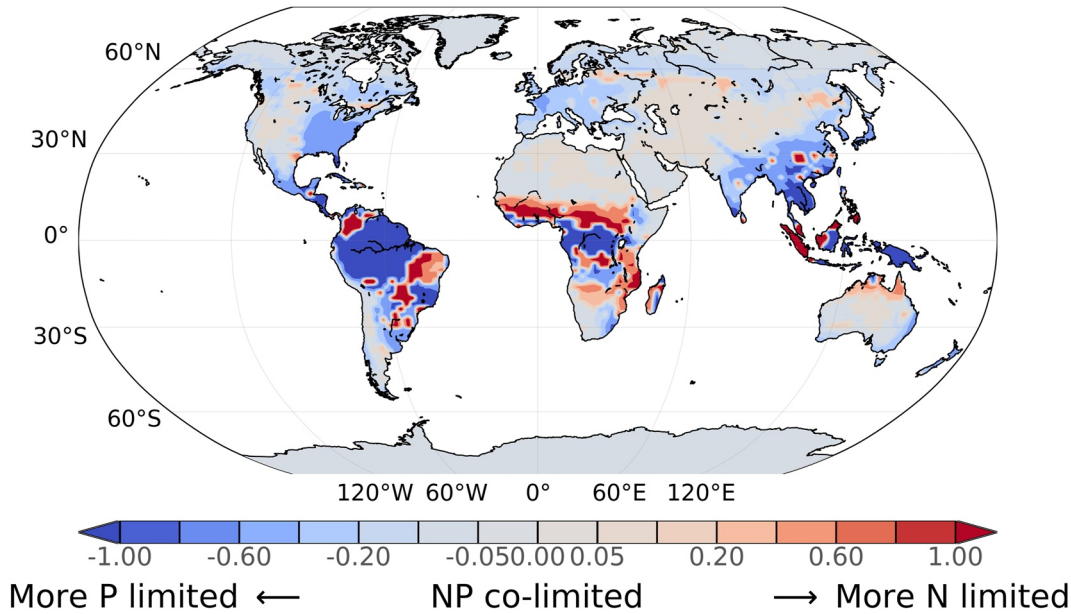

Figure 9. Nearly 80% of the land surface is estimated to be co-limited (gray) by nitrogen (N) and phosphorus (P), with the remaining 20% predominantly limited by either N (red) or P (blue). Global mapping of ELM-FUN3.0 predicted NP limitation for the period 1994–2005 following the stoichiometric homeostasis theory. Global N and P limitations were calculated using the ratio of leaf N and P over the ratio of leaf N and P retranslocation following the stoichiometric homeostasis theory (Sterner & Elser, 2002), in which the demand ratio of N versus P for a mature leaf should be relatively constant to maintain leaf functioning. Estimates indicate that 6.1% of the natural terrestrial land area is limited primarily by N, whereas 13.9% is primarily P limited. The remaining 80% of the land area is co-limited by N and P or weakly limited by either nutrient alone.

spent on P acquisition in evergreen broadleaf and evergreen needleleaf forests, respectively. In deciduous needleleaf forests, retranslocation represents 89% of the total 0.4 ± 0.4 g C m^2 yr^{-1} spent on P acquisition.

3.4. Global Spatial Distribution of Terrestrial N Versus P Limitation

One metric of global N and P limitation is the ratio of leaf N and P to leaf N and P retranslocation–the stoichiometric homeostasis theory (Sterner & Elser, 2002), in which the demand ratio of N versus P for a mature leaf should be relatively constant to maintain leaf functioning (Du et al., 2020). ELM-FUN3.0 indicates a stronger P limitation in the tropics (Figure 9), except over grasslands, which are more N limited (see Figure S4 in Supporting Information S1).

In FUN3.0, leaf N and P retranslocation are related to the environmental cost of N and P by the optimization of C expenditure on retranslocation as the nutrients become more expensive with extraction. Estimates here indicate that 6.1% of the natural terrestrial land area is limited primarily by N, whereas 13.9% is primarily P limited. The remaining 80.0% of the land area is co-limited by N and P or weakly limited by either nutrient alone. Although there is a difference in absolute terms, these results are in alignment with those proposed in Elser et al. (2007) and Du et al. (2020) (Figure S9 in Supporting Information S1), in which a larger part of the global terrestrial land area is more relatively P limited and less significantly limited by N.

4. Discussion

Much of the uncertainty in ESMs projections of the future land C uptake is driven by how these models represent nutrient constraints on NPP (Ciais et al., 2013; Davies-Barnard et al., 2020; Fernández-Martínez et al., 2014; Fisher et al., 2012; Terrer et al., 2019; Wieder et al., 2015a). Using a process model of the dynamics and C economics of N and P acquisition from the environment coupled into ELM addresses part of this uncertainty by dynamically predicting the C costs of N and P acquisition at the same time, noting that book-keeping approaches may provide unreliable results (Sun et al., 2017). Specifically, we evaluated the total amounts and the spatial distributions of N and P acquisition (Figures 5 and 6); the amounts and spatial distributions of C used for N

and P acquisition (Figure 8 and Figure S5 in Supporting Information S1); and changes in NPP as a result of N and P acquisition and allocation at the global scale (Figure 4). ELM-FUN3.0 is able to simulate the distribution of limitation comparably with existing (but limited) empirical estimates (Figure 9 and Figure S9 in Supporting Information S1), as well as the spatial distribution of the C used for acquiring these nutrients (Figure 4b), which provide an important dynamic constraint on predictions of the future land C uptake. In parallel to the addition of new processes, ESMs benefit from systematic benchmarking against observed datasets throughout model development, within initiatives like ILAMB (Collier et al., 2018). Nonetheless, global nutrient cycling benchmarks are limited (e.g., Sun et al. (2020)) and more upscaling exercises from in situ observations are needed (e.g., Du et al. (2020)), as well as the implementation of new technologies to remotely detect information in the rhizosphere (Fisher et al., 2016; Sousa et al., 2021). In this study, we benchmarked all the ELM-FUN model versions (Figures 2,3 and 4) indicating that considering the C costs of N and P acquisition are important for improving the representation of the C cycle.

Accounting for N and N-P limitation lowered historical estimates of NPP by 20% and 50%, respectively (Figure 4a). Our result aligns with a previous study using CMIP5 models for N (Wieder et al., 2015a), but shows a much stronger effect of P on NPP (twice as much). Although previous authors have reported the unlikelihood of the land actually becoming a net source of CO_2 (Brovkin & Goll, 2015), mainly due to changes in mineralization and additional processes governing the recycling of P, our simulations explicitly represent P dynamics and indicate a significant decrease in land C uptake. Similar results were reported for the Amazon, showing that P availability reduces the projected CO_2-induced biomass growth by 50% compared to estimates from C models (Fleischer et al., 2019), although inconclusive based on limited observations (Turner et al., 2018).

ELM-FUN3.0 is on the low end of the CMIP6 NPP range, given that part of the available C is spent on P acquisition. ELM presents a positive GPP bias in comparison to FLUXCOM (0.65 g m^{-2} day^{-1}), also reflected in LAI compared to MODIS (0.95 m^2. m^{-2}), while the model versions with FUN work to reduce the bias, especially in the tropics. Nevertheless, ELM-FUN3.0 reduces tropical and arctic-boreal LAI turning the positive bias into a negative one (−0.17 m^2. m^{-2}). The cumulative Net Biome Production (NBP, Figure S11a in Supporting Information S1) highlights that although none of the model versions are able to capture the C source strengthening up until 1940, and weakening afterwards, all versions are contained within the envelope of observational uncertainty after the 60's.

4.1. Mycorrhizal Association Uncertainty in ELM

It is likely that mycorrhizal associations can explain a large fraction of the variance in plant response to elevated CO_2 (Braghiere, Fisher, et al., 2021; Drake et al., 2011; Kivlin et al., 2013; Orwin et al., 2011; Sulman et al., 2017; Terrer et al., 2016, 2018), because it has been estimated that fungal root symbionts may be responsible for as much as 80% of plant N and P uptake (van der Heijden et al., 2015). Nevertheless, the large-scale spatiotemporal distribution of these plant-fungi associations are highly uncertain (Norby et al., 2017; Sulman et al., 2019). However, in order to enable global simulations with ELM-FUN3.0, an explicit representation of the functional differences between different types of plant symbiotic associations was assumed following the PFT distribution in the original ELM (Table S3 in Supporting Information S1).

The rationale behind this assumption is based upon previously documented geographic distributions of plant symbiosis (Allen et al., 1995; Read, 1991; Shi et al., 2016), where a transition from AM to ECM dominance was reported at single site level observations following a common shift from P to N limitation along increasing latitudes (McGroddy et al., 2004; Reich & Oleksyn, 2004). Although until very recently only a few regional maps of present and past plant symbiotic status were available (Brundrett, 2017; Fisher et al., 2016; Jo et al., 2019; Menzel et al., 2016; Swaty et al., 2016), in the last couple of years a number of different methods were used for extrapolating spatially sparse observations into explicit global maps suitable for applications within ESMs (Braghiere, Fisher, et al., 2021; Soudzilovskaia et al., 2019; Steidinger et al., 2019; Sulman et al., 2019).

Braghiere, Fisher, et al. (2021) show that the map presented in Steidinger et al. (2019) follows the spatial distribution proposed in this study (tropics-AM dominated vs. extra-tropics-ECM dominated), indicating that climate variables are the main drivers of global biogeography of plant-fungi symbioses and that fixed values of mycorrhizal associations can be prescribed following spatial distributions of PFTs in ELM.

Although the C cost of mycorrhizal root uptake of N and P from soil is calculated as a function of availability of soil N and P, and the amount of fine root biomass that can access the nutrient, as described in Equation S3 in Supporting Information S1, currently mycorrhizae do not directly impact availability of N or P, or their interaction with soil organic matter. Further model developments should also include some of these important mechanisms.

4.2. Soil Nutrient Uncertainty in ELM

All nutrient-vegetation models are predicated on the correct functioning of numerous interacting nutrient fluxes in both the soil and vegetation. Here we focused on vegetation processes. The ELM model originated from CLM4.5 with a vertically resolved soil decomposition cascade, which is known for underestimating the production of mineral N resulting in a highly N-limited terrestrial C sink (Koven et al., 2013). In fact, the modeled soil biogeochemistry in ELM-CTC is more sensitive to soil N dynamics than to vegetation biogeochemistry (Tanga & Riley, 2018). Likewise, although ELM considers major P cycle processes, including phosphatase activity, which can relieve P limitation with increasing P demand under elevated CO_2, there are large uncertainties in the availability and dynamics of soil P (Yang et al., 2019). Thus, the soil mineral N and P uptake simulated by ELM-FUN3.0 is likely underestimated. As such, the apparent nutrient limitation down-regulation on NPP we attribute to FUN is in part attributable to the underestimated soil pools already in ELM. However, coupling FUN3.0 with ELM in E3SM opens up new possibilities to explore different acquisition pathways that could alleviate nutrient limitation.

For example, Richter et al. (2006) suggested that occluded P can become available to plants through mycorrhizal associations. The new global implementation of mycorrhizal associations in ELM-FUN3.0 would allow the development and exploration of this hypothesis. Also, Helfenstein et al. (2020) suggests current LSMs largely overestimate mean residence time of inorganic P in soils, as well as the temporal dynamics of P pools vary largely between different soil types, which could explain part of the uncertainty related to soil P. The active role of plants in changing allocation and flexible stoichiometry are not included in these simulations, but could help alleviate P limitation under elevated CO_2 (Buendía et al., 2014). Likewise, new model developments should include environmental mechanisms controlling phosphatase activity (Alewell et al., 2020), alternative methods for plants to access occluded P pools (Schubert et al., 2020), and organic N (Näsholm et al., 2009), such as rhizosphere priming, defined as the increment or suppression of soil organic matter decomposition by live roots and associated rhizosphere microorganisms (Cheng et al., 2014). Further studies are needed to estimate and clarify the relative role of P limitation and acquisition strategies, which can also be further explored with ELM-FUN3.0.

4.3. Further Improvements to ELM-FUN3.0

Many CMIP6 ESMs now consider nutrient cycling (Arora et al., 2020; Jones et al., 2016). Terrestrial C budgets, as well as climate feedbacks, are different from C-only versions because plant C production and allocation are strongly limited by N or P (or both) (Zaehle et al., 2015). Although the newly developed ELM-FUN3.0 expands the abilities of determining interactions in the rhizosphere, including mycorrhizal and direct root uptake, as well as retranslocation of N and P from leaves at the same time, there is room for model development and improvement.

Additional complexity in ESMs, while often justifiable from basic process understanding, has typically been accompanied by an ever-increasing number of parameters (Fisher & Koven, 2020), many of which are poorly constrained by observations (Braghiere, Wang, et al., 2021). New processes can also hinder transparency, robustness, and predictive power due to accumulation of uncertainty (Bonan & Doney, 2018; Braghiere et al., 2019; Franklin et al., 2020; Prentice et al., 2015). In regards to this, there are a few steps to be taken in future ESM development, particularly when referring to C-N-P dynamics in these models, as well as uncertainty of the parameters used in FUN3.0 itself.

While ELM-FUN adds on multiple new model capabilities, inherent model uncertainties encompass parametric and structural uncertainty, which dominate the uncertainty in the land C cycle, while uncertainty in the ocean C cycle is more dominated by data forcing (Lovenduski & Bonan, 2017). Parametric uncertainty in LSMs has been traditionally explored through experimentation with different parameter values in order to test different hypothesis on how these parameters impact predictions (Dagon et al., 2020; Hawkins et al., 2019; Huo et al., 2019; Ricciuto et al., 2018). Originally in FUN, the cost functions (see Equation 3.0 in Supporting Information S1) are a set of parameters that determine the environmental cost of nutrient uptake from soils and retranslocation from

leaves. For instance, root biomass does not necessarily need to be high if nutrient concentration is high, given non-limitation of other factors (Aerts et al., 1991; Fisher et al., 2010). Therefore, the cost parameters are defined to control the balance to which available soil nutrient and fine root biomass impact the C cost uptake (Allen et al., 2020).

For instance, FUN simulates the ability of AM fungi to act as scavengers by reducing the AM C cost parameter relative to that of ECM fungi for N and increase for P to reflect the greater efficiency of different C-intensive strategies (Raven et al., 2018). Likewise, the AM and ECM cost parameters were chosen so that the thresholds in nutrient availability and root biomass mirror empirical shifts in the abundance of these two types of fungi across fertility and latitudinal gradients (Allen et al., 1995; Brzostek et al., 2014; Phillips et al., 2013). This abstraction, however, means that uncertainties associated with the cost functions are large (Fisher et al., 2019).

Fisher et al. (2019) assessed the sensitivity of CLM5 C and N cycles to the FUN cost parameters by conducting one-at-a-time perturbations of the parameters around the default state at four flux tower sites, varying the cost parameters an order of magnitude in each direction from the default value, since reasonable ranges of these parameters are unknown and their physiological controls are poorly understood. For CO_2 and N enrichment experiments, the authors found moderate decline in LAI, NPP, and GPP when cost parameters increased, but highlighted that they do not appear to be a first-order control parameter when compared to allocation parameters in CLM5. Similarly, low values of C costs parameters appeared to reduce the responsiveness of the system to CO_2 fertilization. The cost parameters seem to have a direct impact on fertilization responses illustrating the sensitivity of the model to relatively unconstrained processes. Measuring and modeling these parameters remains an outstanding challenge (Wieder et al., 2021).

Similarly, Braghiere, Fisher, et al. (2021) assessed the sensitivity of CLM5 C and N cycles to different spatial representations of mycorrhizal distributions globally and found differences of up to 8 $TgN.yr^{-1}$ between different maps. It is possible that cost parameters vary following different functions depending on multiple variables other than only latitude and nutrient availability, such as temperature and moisture, species composition, and soils characteristics. Further research is needed in this regard in order to characterize uncertainty and establish a more process-based understanding of parametric controls in FUN.

Although the addition of FUN3.0 into ELM allows new capabilities for simulating global P uptake, including mycorrhizal dynamics, there are a number of processes that are still not represented in the model, such as P retranslocation from all senescing tissues, not only from leaves, soil biological traits and trade-offs to optimize C allocation for P acquisition, such as capturing microbial species composition or changes in soil pH in response to P availability, as well as fixed allocation and resorption of P under soils with limited nutrient availability (Jiang et al., 2019). As incorporation of P dynamics into ESMs develops (Goll et al., 2012; Thum et al., 2019; Wang et al., 2007; Yang, Thornton, et al., 2014, Yang, Post, et al., 2014; Zhu et al., 2019), these models are paving the way for increased inclusion of different P cycle processes (Reed et al., 2015). While large uncertainties in soil P dynamics are due to organic P, inorganic P is a key player in P dynamics (Helfenstein et al., 2020), and a separation of leaf P into organic and inorganic pools would be desirable to improve predictions of photosynthesis (Jiang et al., 2019). Integrating plant parametric adjustments to nutrient use efficiency, such as updating the maximum rate of Rubisco carboxylase activity or the maximum rate of photosynthetic electron transport (Braghiere et al., 2020; Walker et al., 2014), C-N-P ratios of newly formed soil organic matter during decomposition, priming effects on C, N, and P mineralization, and consideration of flexible plant tissue stoichiometry are among the high priority processes needed to be incorporated in further developments of ELM-FUN3.0. The integration of new processes involving C-N-P dynamics can now feasibly be added into the cost structure of FUN3.0, given its highly modular nature (e.g., the cost functions) based on optimality approaches making use of economic concepts, recently advocated as one of the organizing principles to be used in next generation ESMs (Fisher & Koven, 2020; Franklin et al., 2020).

Lastly, the response of N cycling to C fertilization is to some degree a function of the abundance of N fixing plants (Fisher et al., 2019). In ELM-FUN3.0 this is a fixed entity (25% for natural ecosystems). Increasing use of models that resolve vegetation demographics (Koven et al., 2020; Longo et al., 2019) should allow prognostic estimates of how N fixing strategies vary in high CO_2 conditions (Meyerholt et al., 2016).

5. Conclusions

Using a process model of the dynamics and C economics of N and P acquisition from the environment coupled into the E3SM land model, we evaluated the total amounts and the spatial distributions of N and P acquisition; the amounts and spatial distributions of C used for N and P acquisition; and changes in NPP as a result of N and P acquisition and allocation at the global scale. We benchmarked all the ELM-FUN model versions indicating that considering the C costs of N and P acquisition are important for improving the representation of the C and water cycles, and that accounting for N and N-P limitation lowered historical estimates of NPP by 20% and 50%, respectively. Modeled and observed nutrient limitation agreement increases when N and P are considered together (r^2 from 0.73 to 0.83), but the likely nutrient limitation down-regulation on NPP we attribute to FUN is in part attributable to the underestimated soil nutrient pools in ELM.

Conflict of Interest

The authors declare no conflicts of interest relevant to this study.

Data Availability Statement

The E3SM project, code, simulation configurations, model output, and tools to work with the output are described at https://e3sm.org. Instructions on how to get started running E3SM are available at https://e3sm.org/model/running-e3sm/e3sm-quick-start. A patch file and all Python scripts to generate the figures can be found in https://github.com/braghiere/E3SM-FUN3.0/tree/master. The CMIP6 data simulations performed by various modeling groups are available from the CMIP6 archive (https://esgf-node.llnl.gov/search/cmip6). Over land, NPP was used from historical runs. At the CMIP6 archive site searching for a given model, a given experiment, and a given variable name will yield the link to the data set that can be downloaded. Although the average annual value for the period 1994–2005 is used for analysis in this paper, the CMIP6 data archive typically provides monthly values for most variables. The ILAMB package can be downloaded from https://github.com/rubisco-sfa/ILAMB. The ISLSCP II IGBP NPP Output from Terrestrial Biogeochemistry Models data set is available in Cramer et al. (2011). All ILAMB plots with ELM, ELM-FUN2.0, and ELM-FUN3.0 are available from https://braghiere.github.io/ILAMB_ELM_FUN_reduced_v1/. The nutrient limitation data product is available from Fisher et al. (2012).

Acknowledgments
This material is based upon work supported by the U.S. Department of Energy, Office of Science, Office of Biological and Environmental Research, Terrestrial Ecosystem Science program under Award Numbers DE-SC0008317 and DE-SC0016188. Funding was also provided by the NASA IDS program. This research was carried out at the Jet Propulsion Laboratory, California Institute of Technology, under a contract with the National Aeronautics and Space Administration. California Institute of Technology. Government sponsorship acknowledged. Copyright 2022. All rights reserved. This research used resources of the Compute and Data Environment for Science at the Oak Ridge National Laboratory, which is supported by the Office of Science of the U.S. Department of Energy under Contract DE-AC05- 00OR22725. MS was partly supported by the U.S. Department of Energy Office of Science Biological and Environmental Research as part of the Terrestrial Ecosystem Science Program through the Next-Generation Ecosystem Experiments (NGEE) Tropics project. PNNL is operated by Battelle Memorial Institute for the U.S. DOE under contract DE-AC05-76RLO1830. RAF was supported by EU H2020 programs ESM2025 (grant agreement no. 101003536) and 4C (GA 821003). This work was supported by a National Science Foundation Research Coordination Grant (DEB-1754126) to investigate nutrient cycling in terrestrial ecosystems. We would like to thank Benjamin Sulman for helping with ELM, T. Davies-Barnard and Enzai Du for sharing validation data sets, Nate Collier and Min Xu for helping with ILAMB.

References

Adler, R., Sapiano, M., Huffman, G., Wang, J.-J., Gu, G., Bolvin, D., et al. (2018). The global precipitation climatology project (GPCP) monthly analysis (new version 2.3) and a review of 2017 global precipitation. *Atmosphere*, *9*(4), 138. https://doi.org/10.3390/atmos9040138

Aerts, R. (1996). Nutrient resorption from senescing leaves of perennials: Are there general patterns? *Journal of Ecology*, *84*(4), 597. https://doi.org/10.2307/2261481

Aerts, R., Boot, R. G. A., & van der Aart, P. J. M. (1991). The relation between above- and belowground biomass allocation patterns and competitive ability. *Oecologia*, *87*(4), 551–559. https://doi.org/10.1007/BF00320419

Alewell, C., Ringeval, B., Ballabio, C., Robinson, D. A., Panagos, P., & Borrelli, P. (2020). Global phosphorus shortage will be aggravated by soil erosion. *Nature Communications*, *11*(1), 1–12. https://doi.org/10.1038/s41467-020-18326-7

Allen, E. B., Allen, M. F., Helm, D. J., Trappe, J. M., Molina, R., & Rincon, E. (1995). Patterns and regulation of mycorrhizal plant and fungal diversity. *Plant and Soil*, *170*(1), 47–62. https://doi.org/10.1007/BF02183054

Allen, K., Fisher, J. B., Phillips, R. P., Powers, J. S., & Brzostek, E. R. (2020). Modeling the carbon cost of plant nitrogen and phosphorus uptake across temperate and tropical forests. *Frontiers in Forests and Global Change*, *3*, 43. https://doi.org/10.3389/ffgc.2020.00043

Arora, V. K., Katavouta, A., Williams, R. G., Jones, C. D., Brovkin, V., Friedlingstein, P., et al. (2020). Carbon-concentration and carbon-climate feedbacks in CMIP6 models and their comparison to CMIP5 models. *Biogeosciences*, *17*(16), 4173–4222. https://doi.org/10.5194/bg-17-4173-2020

Bloom, A. J., Chapin, F. S., & Mooney, H. A. (1985). Resource limitation in plants–An economic analogy. *Annual Review of Ecology and Systematics*, *16*(1), 363–392. https://doi.org/10.1146/annurev.es.16.110185.002051

Bonan, G. B., & Doney, S. C. (2018). Climate, ecosystems, and planetary futures: The challenge to predict life in Earth system models. *Science*, *359*(6375), eaam8328. https://doi.org/10.1126/science.aam8328

Bonan, G. B., Lawrence, P. J., Oleson, K. W., Levis, S., Jung, M., Reichstein, M., et al. (2011). Improving canopy processes in the community land model version 4 (CLM4) using global flux fields empirically inferred from FLUXNET data. *Journal of Geophysical Research*, *116*(G2), G02014. https://doi.org/10.1029/2010JG001593

Braghiere, R. K., Fisher, J. B., Fisher, R. A., Shi, M., Steidinger, B. S., Sulman, B. N., et al. (2021). Mycorrhizal distributions impact global patterns of carbon and nutrient cycling. *Geophysical Research Letters*, *48*(19). https://doi.org/10.1029/2021GL094514

Braghiere, R. K., Gérard, F., Evers, J. B., Pradal, C., & Pagès, L. (2020). Simulating the effects of water limitation on plant biomass using a 3D functional–structural plant model of shoot and root driven by soil hydraulics. *Annals of Botany*, *126*(4), 713–728. https://doi.org/10.1093/aob/mcaa059

Braghiere, R. K., Quaife, T., Black, E., He, L., & Chen, J. M. (2019). Underestimation of global photosynthesis in Earth system models due to representation of vegetation structure. *Global Biogeochemical Cycles*, *33*(11), 1358–1369. https://doi.org/10.1029/2018GB006135

Braghiere, R. K., Wang, Y., Doughty, R., Sousa, D., Magney, T., Widlowski, J.-L., et al. (2021). Accounting for canopy structure improves hyperspectral radiative transfer and sun-induced chlorophyll fluorescence representations in a new generation Earth System model. *Remote Sensing of Environment*, *261*, 112497. https://doi.org/10.1016/j.rse.2021.112497

Brovkin, V., & Goll, D. (2015). Land unlikely to become large carbon source. *Nature Geoscience*, *8*(12), 893. https://doi.org/10.1038/ngeo2598

Brundrett, M. C. (2017). Distribution and evolution of mycorrhizal types and other specialised roots in Australia (pp. 361–394). https://doi.org/10.1007/978-3-319-56363-3_17

Brzostek, E. R., Dragoni, D., Brown, Z. A., & Phillips, R. P. (2015). Mycorrhizal type determines the magnitude and direction of root-induced changes in decomposition in a temperate forest. *New Phytologist*, *206*(4), 1274–1282. https://doi.org/10.1111/nph.13303

Brzostek, E. R., Fisher, J. B., & Phillips, R. P. (2014). Modeling the carbon cost of plant nitrogen acquisition: Mycorrhizal trade-offs and multipath resistance uptake improve predictions of retranslocation. *Journal of Geophysical Research: Biogeosciences*, *119*(8), 1684–1697. https://doi.org/10.1002/2014JG002660

Buendía, C., Arens, S., Hickler, T., Higgins, S. I., Porada, P., & Kleidon, A. (2014). On the potential vegetation feedbacks that enhance phosphorus availability–Insights from a process-based model linking geological and ecological timescales. *Biogeosciences*, *11*(13), 3661–3683. https://doi.org/10.5194/bg-11-3661-2014

Burrows, S. M., Maltrud, M., Yang, X., Zhu, Q., Jeffery, N., Shi, X., et al. (2020). The DOE E3SM v1.1 biogeochemistry configuration: Description and simulated ecosystem-climate responses to historical changes in forcing. *Journal of Advances in Modeling Earth Systems*, *12*(9). https://doi.org/10.1029/2019MS001766

Cai, X., Yang, Z.-L., Fisher, J. B., Zhang, X., Barlage, M., & Chen, F. (2016). Integration of nitrogen dynamics into the Noah-MP land surface model v1.1 for climate and environmental predictions. *Geoscientific Model Development*, *9*(1), 1–15. https://doi.org/10.5194/gmd-9-1-2016

Caldwell, P. M., Mametjanov, A., Tang, Q., Van Roekel, L. P., Golaz, J. C., Lin, W., et al. (2019). The DOE E3SM coupled model version 1: Description and results at high resolution. *Journal of Advances in Modeling Earth Systems*, *11*(12), 4095–4146. https://doi.org/10.1029/2019MS001870

Campioli, M., Vicca, S., Luyssaert, S., Bilcke, J., Ceschia, E., Chapin, F. S., III, et al. (2015). Biomass production efficiency controlled by management in temperate and boreal ecosystems. *Nature Geoscience*, *8*(11), 843–846. https://doi.org/10.1038/ngeo2553

Chapin, F. S., Vitousek, P. M., & Van Cleve, K. (1986). The nature of nutrient limitation in plant communities. *The American Naturalist*, *127*(1), 48–58. https://doi.org/10.1086/284466

Chapin, F. S., Zavaleta, E. S., Eviner, V. T., Naylor, R. L., Vitousek, P. M., Reynolds, H. L., et al. (2000). Consequences of changing biodiversity. *Nature*, *405*(6783), 234–242. Nature Publishing Group. https://doi.org/10.1038/35012241

Cheng, W., Parton, W. J., Gonzalez-Meler, M. A., Phillips, R., Asao, S., Mcnickle, G. G., et al. (2014). Synthesis and modeling perspectives of rhizosphere priming. *New Phytologist*, *201*(1), 31–44. https://doi.org/10.1111/NPH.12440

Ciais, P., Sabine, C., Bala, G., Bopp, L., Brovkin, V., Canadell, J., et al. (2013). Carbon and other biogeochemical cycles. In T. F. Stocker, D. Qin, G.-K. Plattner, M. Tignor, S. K. Allen, J. Boschung, et al. (Eds.), *Climate change 2013–the physical science basis* (pp. 465–570). Cambridge University Press.

Collier, N., Hoffman, F. M., Lawrence, D. M., Keppel-Aleks, G., Koven, C. D., Riley, W. J., et al. (2018). The international land model benchmarking (ILAMB) system: Design, theory, and implementation. *Journal of Advances in Modeling Earth Systems*, *10*(11), 2731–2754. https://doi.org/10.1029/2018MS001354

Cramer, W., Kicklighter, D. W., Bondeau, A., Moore, B., Churkina, G., Nemry, B., et al. (1999). Comparing global models of terrestrial net primary productivity (NPP): Overview and key results. *Global Change Biology*, *5*(S1), 1–15. https://doi.org/10.1046/j.1365-2486.1999.00009.x

Cramer, W. P., Hall, F. G., Collatz, G. J., Meeson, B. W., Los, S. O., Brown De Colstoun, E., & Landis, D. R. (2011). *ISLSCP II IGBP NPP output from terrestrial biogeochemistry models*. ORNL DAAC. https://doi.org/10.3334/ORNLDAAC/1027

Dagon, K., Sanderson, B. M., Fisher, R. A., & Lawrence, D. M. (2020). A machine learning approach to emulation and biophysical parameter estimation with the community land model, version 5. *Advances in Statistical Climatology, Meteorology and Oceanography*, *6*(2), 223–244. https://doi.org/10.5194/ascmo-6-223-2020

Davies-Barnard, T., & Friedlingstein, P. (2020). The global distribution of biological nitrogen fixation in terrestrial natural ecosystems. *Global Biogeochemical Cycles*, *34*(3). https://doi.org/10.1029/2019GB006387

Davies-Barnard, T., Meyerholt, J., Zaehle, S., Friedlingstein, P., Brovkin, V., Fan, Y., et al. (2020). Nitrogen cycling in CMIP6 land surface models: Progress and limitations. *Biogeosciences*, *17*(20), 5129–5148. https://doi.org/10.5194/bg-17-5129-2020

De Kauwe, M. G., Disney, M. I., Quaife, T., Lewis, P., & Williams, M. (2011). An assessment of the MODIS collection 5 leaf area index product for a region of mixed coniferous forest. *Remote Sensing of Environment*, *115*(2), 767–780. https://doi.org/10.1016/j.rse.2010.11.004

Dickinson, R. E., Berry, J. A., Bonan, G. B., Collatz, G. J., Field, C. B., Fung, I. Y., et al. (2002). Nitrogen controls on climate model evapotranspiration. *Journal of Climate*, *15*(3), 278–295. https://doi.org/10.1175/1520-0442(2002)015<0278:ncocme>2.0.co;2

Dirmeyer, P. A., Gao, X., Zhao, M., Guo, Z., Oki, T., & Hanasaki, N. (2006). GSWP-2: Multimodel analysis and implications for our perception of the land surface. *Bulletin of the American Meteorological Society*, *87*(10), 1381–1397. https://doi.org/10.1175/BAMS-87-10-1381

Drake, J. E., Gallet-Budynek, A., Hofmockel, K. S., Bernhardt, E. S., Billings, S. A., Jackson, R. B., et al. (2011). Increases in the flux of carbon belowground stimulate nitrogen uptake and sustain the long-term enhancement of forest productivity under elevated CO_2. *Ecology Letters*, *14*(4), 349–357. https://doi.org/10.1111/j.1461-0248.2011.01593.x

Du, E., Terrer, C., Pellegrini, A. F. A., Ahlström, A., van Lissa, C. J., Zhao, X., et al. (2020). Global patterns of terrestrial nitrogen and phosphorus limitation. *Nature Geoscience*, *13*(3), 221–226. https://doi.org/10.1038/s41561-019-0530-4

Elser, J. J., Bracken, M. E. S., Cleland, E. E., Gruner, D. S., Harpole, W. S., Hillebrand, H., et al. (2007). Global analysis of nitrogen and phosphorus limitation of primary producers in freshwater, marine and terrestrial ecosystems. *Ecology Letters*, *10*(12), 1135–1142. https://doi.org/10.1111/j.1461-0248.2007.01113.x

Eyring, V., Bony, S., Meehl, G. A., Senior, C. A., Stevens, B., Stouffer, R. J., & Taylor, K. E. (2016). Overview of the coupled model intercomparison project phase 6 (CMIP6) experimental design and organization. *Geoscientific Model Development*, *9*(5), 1937–1958. https://doi.org/10.5194/gmd-9-1937-2016

Fay, P. A., Prober, S. M., Harpole, W. S., Knops, J. M. H., Bakker, J. D., Borer, E. T., et al. (2015). Grassland productivity limited by multiple nutrients. *Nature Plants*, *1*(7), 1–5. https://doi.org/10.1038/nplants.2015.80

Fernández-Martínez, M., Vicca, S., Janssens, I. A., Sardans, J., Luyssaert, S., Campioli, M., et al. (2014). Nutrient availability as the key regulator of global forest carbon balance. *Nature Climate Change*, *4*(6), 471–476. https://doi.org/10.1038/nclimate2177

Fisher, J. B., Badgley, G., & Blyth, E. (2012). Global nutrient limitation in terrestrial vegetation. *Global Biogeochemical Cycles*, *26*(3), 2011GB004252. https://doi.org/10.1029/2011GB004252

Fisher, J. B., Sitch, S., Malhi, Y., Fisher, R. A., Huntingford, C., & Tan, S.-Y. (2010). Carbon cost of plant nitrogen acquisition: A mechanistic, globally applicable model of plant nitrogen uptake, retranslocation, and fixation. *Global Biogeochemical Cycles*, *24*(1). https://doi.org/10.1029/2009gb003621

Fisher, J. B., Sweeney, S., Brzostek, E. R., Evans, T. P., Johnson, D. J., Myers, J. A., et al. (2016). Tree-mycorrhizal associations detected remotely from canopy spectral properties. *Global Change Biology*, *22*(7), 2596–2607. https://doi.org/10.1111/gcb.13264

Fisher, R. A., & Koven, C. D. (2020). Perspectives on the future of land surface models and the challenges of representing complex terrestrial systems. *Journal of Advances in Modeling Earth Systems*, *12*(4). https://doi.org/10.1029/2018ms001453

Fisher, R. A., Wieder, W. R., Sanderson, B. M., Koven, C. D., Oleson, K. W., Xu, C., et al. (2019). Parametric controls on vegetation responses to biogeochemical forcing in the CLM5. *Journal of Advances in Modeling Earth Systems*, *11*(9), 2879–2895. https://doi.org/10.1029/2019MS001609

Fleischer, K., Rammig, A., De Kauwe, M. G., Walker, A. P., Domingues, T. F., Fuchslueger, L., et al. (2019). Amazon forest response to CO_2 fertilization dependent on plant phosphorus acquisition. *Nature Geoscience*, *12*(9), 736–741. https://doi.org/10.1038/s41561-019-0404-9

Franklin, O., Harrison, S. P., Dewar, R., Farrior, C. E., Brännström, Å., Dieckmann, U., et al. (2020). Organizing principles for vegetation dynamics. *Nature Plants*, *6*(5), 444–453. https://doi.org/10.1038/s41477-020-0655-x

Friedlingstein, P., Cox, P., Betts, R., Bopp, L., von Bloh, W., Brovkin, V., et al. (2006). Climate-carbon cycle feedback analysis: Results from the C4MIP model intercomparison. *Journal of Climate*, *19*(14), 3337–3353. https://doi.org/10.1175/JCLI3800.1

Friedlingstein, P., Jones, M. W., O' Sullivan, M., Andrew, R. M., Hauck, J., Peters, G. P., et al. (2019). Global carbon budget 2019. *Earth System Science Data*, *11*(4), 1783–1838. https://doi.org/10.5194/essd-11-1783-2019

Friedlingstein, P., Meinshausen, M., Arora, V. K., Jones, C. D., Anav, A., Liddicoat, S. K., & Knutti, R. (2014). Uncertainties in CMIP5 climate projections due to carbon cycle feedbacks. *Journal of Climate*, *27*(2), 511–526. https://doi.org/10.1175/JCLI-D-12-00579.1

Galbraith, D., Malhi, Y., Affum-Baffoe, K., Castanho, A. D. A., Doughty, C. E., Fisher, R. A., et al. (2013). Residence times of woody biomass in tropical forests. *Plant Ecology & Diversity*, *6*(1), 139–157. https://doi.org/10.1080/17550874.2013.770578

Golaz, J., Caldwell, P. M., Van Roekel, L. P., Petersen, M. R., Tang, Q., Wolfe, J. D., et al. (2019). The DOE E3SM coupled model version 1: Overview and evaluation at standard resolution. *Journal of Advances in Modeling Earth Systems*, *11*(7), 2089–2129. https://doi.org/10.1029/2018MS001603

Goll, D. S., Brovkin, V., Parida, B. R., Reick, C. H., Kattge, J., Reich, P. B., et al. (2012). Nutrient limitation reduces land carbon uptake in simulations with a model of combined carbon, nitrogen and phosphorus cycling. *Biogeosciences*, *9*(9), 3547–3569. https://doi.org/10.5194/bg-9-3547-2012

Guignard, M. S., Leitch, A. R., Acquisti, C., Eizaguirre, C., Elser, J. J., Hessen, D. O., et al. (2017). Impacts of nitrogen and phosphorus: From genomes to natural ecosystems and agriculture. *Frontiers in Ecology and Evolution*, *5*. https://doi.org/10.3389/fevo.2017.00070

Harris, I., Jones, P. D., Osborn, T. J., & Lister, D. H. (2014). Updated high-resolution grids of monthly climatic observations–The CRU TS3.10 Dataset. *International Journal of Climatology*, *34*(3), 623–642. https://doi.org/10.1002/joc.3711

Hawkins, L. R., Rupp, D. E., McNeall, D. J., Li, S., Betts, R. A., Mote, P. W., et al. (2019). Parametric sensitivity of vegetation dynamics in the TRIFFID model and the associated uncertainty in projected climate change impacts on western U.S. Forests. *Journal of Advances in Modeling Earth Systems*, *11*(8), 2787–2813. https://doi.org/10.1029/2018MS001577

Helfenstein, J., Pistocchi, C., Oberson, A., Tamburini, F., Goll, D. S., & Frossard, E. (2020). Estimates of mean residence times of phosphorus in commonly considered inorganic soil phosphorus pools. *Biogeosciences*, *17*(2), 441–454. https://doi.org/10.5194/BG-17-441-2020

Hobbie, E. A. (2006). Carbon allocation to ectomycorrhizal fungi correlates with belowground allocation in culture studies. *Ecology*, *87*(3), 563–569. https://doi.org/10.1890/05-0755

Hobbie, E. A., & Hobbie, J. E. (2008). Natural abundance of ^{15}N in nitrogen-limited forests and tundra can estimate nitrogen cycling through mycorrhizal fungi: A review. *Ecosystems*, *11*(5), 815–830. https://doi.org/10.1007/S10021-008-9159-7

Hoffman, F. M., Randerson, J. T., Arora, V. K., Bao, Q., Cadule, P., Ji, D., et al. (2014). Causes and implications of persistent atmospheric carbon dioxide biases in Earth system models. *Journal of Geophysical Research: Biogeosciences*, *119*(2), 141–162. https://doi.org/10.1002/2013JG002381

Högberg, M. N., & Högberg, P. (2002). Extramatrical ectomycorrhizal mycelium contributes one-third of microbial biomass and produces, together with associated roots, half the dissolved organic carbon in a forest soil. *New Phytologist*, *154*(3), 791–795. https://doi.org/10.1046/j.1469-8137.2002.00417.x

Holm, J. A., Knox, R. G., Zhu, Q., Fisher, R. A., Koven, C. D., Nogueira Lima, A. J., et al. (2020). The central Amazon biomass sink under current and future atmospheric CO_2: Predictions from big-leaf and demographic vegetation models. *Journal of Geophysical Research: Biogeosciences*, *125*(3). https://doi.org/10.1029/2019JG005500

Hou, E., Luo, Y., Kuang, Y., Chen, C., Lu, X., Jiang, L., et al. (2020). Global meta-analysis shows pervasive phosphorus limitation of aboveground plant production in natural terrestrial ecosystems. *Nature Communications*, *11*(1), 1–9. https://doi.org/10.1038/s41467-020-14492-w

Huo, X., Gupta, H., Niu, G. Y., Gong, W., & Duan, Q. (2019). Parameter sensitivity analysis for computationally intensive spatially distributed dynamical environmental systems models. *Journal of Advances in Modeling Earth Systems*, *11*(9), 2896–2909. https://doi.org/10.1029/2018MS001573

Hurtt, G. C. (2018). Final report: Enabling land-use in E3SM land model. https://doi.org/10.2172/1430711

Jiang, J., Moore, J. A. M., Priyadarshi, A., & Classen, A. T. (2017). Plant-mycorrhizal interactions mediate plant community coexistence by altering resource demand. *Ecology*, *98*(1), 187–197. https://doi.org/10.1002/ecy.1630

Jiang, M., Caldararu, S., Zaehle, S., Ellsworth, D. S., & Medlyn, B. E. (2019). Towards a more physiological representation of vegetation phosphorus processes in land surface models. *New Phytologist*, *222*(3), 1223–1229. https://doi.org/10.1111/nph.15688

Jo, I., Fei, S., Oswalt, C. M., Domke, G. M., & Phillips, R. P. (2019). Shifts in dominant tree mycorrhizal associations in response to anthropogenic impacts. *Science Advances*, *5*(4), eaav6358. https://doi.org/10.1126/sciadv.aav6358

Jones, C. D., Arora, V., Friedlingstein, P., Bopp, L., Brovkin, V., Dunne, J., et al. (2016). C4MIP–The coupled climate–carbon cycle model intercomparison project: Experimental protocol for CMIP6. *Geoscientific Model Development*, *9*(8), 2853–2880. https://doi.org/10.5194/gmd-9-2853-2016

Jung, M., Koirala, S., Weber, U., Ichii, K., Gans, F., Camps-Valls, G., et al. (2019). The FLUXCOM ensemble of global land-atmosphere energy fluxes. *Scientific Data*, *6*(1), 1–14. https://doi.org/10.1038/s41597-019-0076-8

Jung, M., Schwalm, C., Migliavacca, M., Walther, S., Camps-Valls, G., Koirala, S., et al. (2020). Scaling carbon fluxes from eddy covariance sites to globe: Synthesis and evaluation of the FLUXCOM approach. *Biogeosciences*, *17*(5), 1343–1365. https://doi.org/10.5194/bg-17-1343-2020

Kato, S., Rose, F. G., Rutan, D. A., Thorsen, T. J., Loeb, N. G., Doelling, D. R., et al. (2018). Surface irradiances of edition 4.0 Clouds and the Earth's radiant energy system (CERES) energy balanced and filled (EBAF) data product. *Journal of Climate*, *31*(11), 4501–4527. https://doi.org/10.1175/JCLI-D-17-0523.1

Kivlin, S. N., Emery, S. M., & Rudgers, J. A. (2013). Fungal symbionts alter plant responses to global change. *American Journal of Botany*, *100*(7), 1445–1457. https://doi.org/10.3732/ajb.1200558

Koven, C. D., Knox, R. G., Fisher, R. A., Fisher, R. A., Chambers, J. Q., Chambers, J. Q., et al. (2020). Benchmarking and parameter sensitivity of physiological and vegetation dynamics using the functionally assembled terrestrial ecosystem simulator (FATES) at Barro Colorado Island, Panama. *Biogeosciences*, *17*(11), 3017–3044. https://doi.org/10.5194/bg-17-3017-2020

Koven, C. D., Riley, W. J., Subin, Z. M., Tang, J. Y., Torn, M. S., Collins, W. D., et al. (2013). The effect of vertically resolved soil biogeochemistry and alternate soil C and N models on C dynamics of CLM4. *Biogeosciences*, *10*(11), 7109–7131. https://doi.org/10.5194/bg-10-7109-2013

Kowalczyk, E., Stevens, L., Law, R., Dix, M., Wang, Y., Harman, I., et al. (2013). The land surface model component of ACCESS: Description and impact on the simulated surface climatology. *Australian Meteorological and Oceanographic Journal*, *63*(1), 65–82. https://doi.org/10.22499/2.6301.005

Lamarque, J. F., Kiehl, J. T., Brasseur, G. P., Butler, T., Cameron-Smith, P., Collins, W. D., et al. (2005). Assessing future nitrogen deposition and carbon cycle feedback using a multimodel approach: Analysis of nitrogen deposition. *Journal of Geophysical Research - D: Atmospheres*, *110*(19), 1–21. https://doi.org/10.1029/2005JD005825

Lawrence, D. M., Fisher, R. A., Koven, C. D., Oleson, K. W., Swenson, S. C., Bonan, G., et al. (2019). The community land model version 5: Description of new features, benchmarking, and impact of forcing uncertainty. *Journal of Advances in Modeling Earth Systems*, *11*(12), 4245–4287. https://doi.org/10.1029/2018MS001583

Lawrence, D. M., Hurtt, G. C., Arneth, A., Brovkin, V., Calvin, K. V., Jones, A. D., et al. (2016). The land use model intercomparison project (LUMIP) contribution to CMIP6: Rationale and experimental design. *Geoscientific Model Development*, *9*(9), 2973–2998. https://doi.org/10.5194/gmd-9-2973-2016

LeBauer, D. S., & Treseder, K. K. (2008). Nitrogen limitation of net primary productivity in terrestrial ecosystems is globally distributed. *Ecology*, *89*(2), 371–379. https://doi.org/10.1890/06-2057.1

Le Quéré, C., Andrew, R. M., Canadell, J. G., Sitch, S., Ivar Korsbakken, J., Peters, G. P., et al. (2016). Global carbon budget 2016. *Earth System Science Data*, *8*(2), 605–649. https://doi.org/10.5194/essd-8-605-2016

Loeb, N. G., Doelling, D. R., Wang, H., Su, W., Nguyen, C., Corbett, J. G., et al. (2018). Clouds and the Earth's radiant energy system (CERES) energy balanced and filled (EBAF) top-of-atmosphere (TOA) edition-4.0 data product. *Journal of Climate*, *31*(2), 895–918. https://doi.org/10.1175/JCLI-D-17-0208.1

Longo, M., Knox, R. G., Levine, N. M., Swann, A. L. S., Medvigy, D. M., Dietze, M. C., et al. (2019). The biophysics, ecology, and biogeochemistry of functionally diverse, vertically and horizontally heterogeneous ecosystems: The ecosystem demography model, version 2.2-Part 2: Model evaluation for tropical South America. *Geoscientific Model Development*, *12*(10), 4347–4374. https://doi.org/10.5194/gmd-12-4347-2019

Lötscher, M., Klumpp, K., & Schnyder, H. (2004). Growth and maintenance respiration for individual plants in hierarchically structured canopies of *Medicago sativa* and *Helianthus annuus*: The contribution of current and old assimilates. *New Phytologist*, *164*(2), 305–316. https://doi.org/10.1111/J.1469-8137.2004.01170.X

Lovenduski, N. S., & Bonan, G. B. (2017). Reducing uncertainty in projections of terrestrial carbon uptake. *Environmental Research Letters*, *12*(4), 044020. https://doi.org/10.1088/1748-9326/aa66b8

Mahowald, N. M., Baker, A. R., Bergametti, G., Brooks, N., Duce, R. A., Jickells, T. D., et al. (2005). Atmospheric global dust cycle and iron inputs to the ocean. *Global Biogeochemical Cycles*, *19*(4). https://doi.org/10.1029/2004GB002402

Malhi, Y., Aragão, L. E. O. C., Metcalfe, D. B., Paiva, R., Quesada, C. A., Almeida, S., et al. (2009). Comprehensive assessment of carbon productivity, allocation and storage in three Amazonian forests. *Global Change Biology*, *15*(5), 1255–1274. https://doi.org/10.1111/J.1365-2486.2008.01780.X

Martens, B., Miralles, D. G., Lievens, H., van der Schalie, R., de Jeu, R. A. M., Fernández-Prieto, D., et al. (2017). GLEAM v3: Satellite-based land evaporation and root-zone soil moisture. *Geoscientific Model Development*, *10*(5), 1903–1925. https://doi.org/10.5194/gmd-10-1903-2017

McGroddy, M. E., Daufresne, T., & Hedin, L. O. (2004). Scaling of C:N:P stoichiometry in forests worldwide: Implications of terrestrial redfield-type ratios. *Ecology*, *85*(9), 2390–2401. https://doi.org/10.1890/03-0351

Meier, R., Davin, E. L., Lejeune, Q., Hauser, M., Li, Y., Martens, B., et al. (2018). Evaluating and improving the Community Land Model's sensitivity to land cover. *Biogeosciences*, *15*, 4731–4757. https://doi.org/10.5194/bg-15-4731-2018

Menzel, A., Hempel, S., Manceur, A. M., Götzenberger, L., Moora, M., Rillig, M. C., et al. (2016). Distribution patterns of arbuscular mycorrhizal and non-mycorrhizal plant species in Germany. *Perspectives in Plant Ecology, Evolution and Systematics*, *21*, 78–88. https://doi.org/10.1016/j.ppees.2016.06.002

Metcalfe, D. B., Ricciuto, D., Palmroth, S., Campbell, C., Hurry, V., Mao, J., et al. (2017). Informing climate models with rapid chamber measurements of forest carbon uptake. *Global Change Biology*, *23*(5), 2130–2139. https://doi.org/10.1111/gcb.13451

Meyerholt, J., Zaehle, S., & Smith, M. J. (2016). Variability of projected terrestrial biosphere responses to elevated levels of atmospheric CO_2 due to uncertainty in biological nitrogen fixation. *Biogeosciences*, *13*(5), 1491–1518. https://doi.org/10.5194/bg-13-1491-2016

Näsholm, T., Kielland, K., & Ganeteg, U. (2009). Uptake of organic nitrogen by plants. *New Phytologist*, *182*(1), 31–48. https://doi.org/10.1111/J.1469-8137.2008.02751.X

Niu, G.-Y., Yang, Z.-L., Mitchell, K. E., Chen, F., Ek, M. B., Barlage, M., et al. (2011). The community Noah land surface model with multiparameterization options (Noah-MP): 1. Model description and evaluation with local-scale measurements. *Journal of Geophysical Research*, *116*(D12), D12109. https://doi.org/10.1029/2010JD015139

Norby, R. J., De Kauwe, M. G., Walker, A. P., Werner, C., Zaehle, S., & Zak, D. R. (2017). Comment on mycorrhizal association as a primary control of the CO_2 fertilization effect. *Science*, *355*(6323), 358. https://doi.org/10.1126/science.aai7976

Oleson, K., Lawrence, D. M., Bonan, G. B., Drewniak, B., Huang, M., Koven, C. D., et al. (2013). Technical description of version 4.5 of the community land model (CLM). https://doi.org/10.5065/D6RR1W7M

Oleson, K. W., Lawrence, D. M., Gordon, B., Flanner, M. G., Kluzek, E., Peter, J., et al. (2010). Technical description of version 4.0 of the community land model (CLM). *NCAR/TN-478+STR NCAR Technical Note*. https://doi.org/10.5065/D6RR1W7M

Orwin, K. H., Kirschbaum, M. U. F., St John, M. G., & Dickie, I. A. (2011). Organic nutrient uptake by mycorrhizal fungi enhances ecosystem carbon storage: A model-based assessment. *Ecology Letters*, *14*(5), 493–502. https://doi.org/10.1111/j.1461-0248.2011.01611.x

Ostle, N. J., Smith, P., Fisher, R., Ian Woodward, F., Fisher, J. B., Smith, J. U., et al. (2009). Integrating plant-soil interactions into global carbon cycle models. *Journal of Ecology*, *97*(5), 851–863. John Wiley & Sons, Ltd. https://doi.org/10.1111/j.1365-2745.2009.01547.x

Parniske, M. (2008). Arbuscular mycorrhiza: The mother of plant root endosymbioses. *Nature Reviews Microbiology*, *6*(10), 763–775. https://doi.org/10.1038/nrmicro1987

Pastorello, G., Trotta, C., Canfora, E., Chu, H., Christianson, D., Cheah, Y.-W., et al. (2020). The FLUXNET2015 dataset and the ONEFlux processing pipeline for eddy covariance data. *Scientific Data*, *7*, 1–27. https://doi.org/10.1038/s41597-020-0534-3

Peng, J., Wang, Y.-P., Houlton, B. Z., Dan, L., Pak, B., & Tang, X. (2020). Global carbon sequestration is highly sensitive to model-based formulations of nitrogen fixation. *Global Biogeochemical Cycles*, *34*(1), e2019GB006296. https://doi.org/10.1029/2019GB006296

Phillips, R. P., Brzostek, E., & Midgley, M. G. (2013). The mycorrhizal-associated nutrient economy: A new framework for predicting carbon-nutrient couplings in temperate forests. *New Phytologist*, *199*(1), 41–51. https://doi.org/10.1111/nph.12221

Prentice, I. C., Liang, X., Medlyn, B. E., & Wang, Y.-P. (2015). Reliable, robust and realistic: The three R's of next-generation land-surface modelling. *Atmospheric Chemistry and Physics*, *15*(10), 5987–6005. https://doi.org/10.5194/acp-15-5987-2015

Rastetter, E. B., Ågren, G. I., & Shaver, G. R. (1997). Responses of N-limited ecosystems to increased CO_2: A balanced-nutrition, coupled-element-cycles model. *Ecological Application*s, 7(2), 444–460. https://doi.org/10.2307/2269511

Rastetter, E. B., Vitousek, P. M., Field, C., Shaver, G. R., Herbert, D., & Gren, G. I. (2001). Resource optimization and symbiotic nitrogen fixation. *Ecosystems*, *4*(4), 369–388. https://doi.org/10.1007/s10021-001-0018-z

Raven, J. A., Lambers, H., Smith, S. E., & Westoby, M. (2018). Costs of acquiring phosphorus by vascular land plants: Patterns and implications for plant coexistence. *New Phytologist*, *217*(4), 1420–1427. https://doi.org/10.1111/nph.14967

Read, D. J. (1991). Mycorrhizas in ecosystems. *Experientia*, *47*(4), 376–391. https://doi.org/10.1007/BF01972080

Reed, S. C., Townsend, A. R., Davidson, E. A., & Cleveland, C. C. (2012). Stoichiometric patterns in foliar nutrient resorption across multiple scales. *New Phytologist*, *196*(1), 173–180. https://doi.org/10.1111/j.1469-8137.2012.04249.x

Reed, S. C., Yang, X., & Thornton, P. E. (2015). Incorporating phosphorus cycling into global modeling efforts: A worthwhile, tractable endeavor. *New Phytologist*, *208*(2), 324–329. https://doi.org/10.1111/nph.13521

Reich, P. B., & Oleksyn, J. (2004). Global patterns of plant leaf N and P in relation to temperature and latitude. *Proceedings of the National Academy of Sciences of the United States of America*, *101*(30), 11001–11006. https://doi.org/10.1073/pnas.0403588101

Riahi, K., van Vuuren, D. P., Kriegler, E., Edmonds, J., O'Neill, B. C., Fujimori, S., et al. (2017). The Shared Socioeconomic Pathways and their energy, land use, and greenhouse gas emissions implications: An overview. *Global Environmental Change*, *42*, 153–168. https://doi.org/10.1016/j.gloenvcha.2016.05.009

Ricciuto, D., Sargsyan, K., & Thornton, P. (2018). The impact of parametric uncertainties on biogeochemistry in the E3SM land model. *Journal of Advances in Modeling Earth Systems*, *10*(2), 297–319. https://doi.org/10.1002/2017MS000962

Richter, D. D., Allen, H. L., Li, J., Markewitz, D., & Raikes, J. (2006). Bioavailability of slowly cycling soil phosphorus: Major restructuring of soil P fractions over four decades in an aggrading forest. *Oecologia*, *150*(2), 259–271. https://doi.org/10.1007/s00442-006-0510-4

Riley, W. J., Zhu, Q., & Tang, J. Y. (2018). Weaker land–climate feedbacks from nutrient uptake during photosynthesis-inactive periods. *Nature Climate Change*, *8*(11), 1002–1006. https://doi.org/10.1038/s41558-018-0325-4

Running, S. W., Nemani, R. R., Heinsch, F. A., Zhao, M., Reeves, M., & Hashimoto, H. (2004). A continuous satellite-derived measure of global terrestrial primary production. *BioScience*, *54*(6), 547. https://doi.org/10.1641/0006-3568(2004)054[0547:acsmog]2.0.co;2

Running, S. W., & Zhao, M. (2015). User's guide daily GPP and annual NPP (MOD17A2/A3) products NASA Earth observing system MODIS land algorithm.

Saatchi, S. S., Harris, N. L., Brown, S., Lefsky, M., Mitchard, E. T. A., Salas, W., et al. (2011). Benchmark map of forest carbon stocks in tropical regions across three continents. *Proceedings of the National Academy of Sciences of the United States of America*, *108*(24), 9899–9904. https://doi.org/10.1073/pnas.1019576108

Schimel, D., Stephens, B. B., & Fisher, J. B. (2015). Effect of increasing CO_2 on the terrestrial carbon cycle. *Proceedings of the National Academy of Sciences of the United States of America*, *112*(2), 436–441. https://doi.org/10.1073/pnas.1407302112

Schubert, S., Steffens, D., & Ashraf, I. (2020). Is occluded phosphate plant-available? *Journal of Plant Nutrition and Soil Science*, *183*(3), 338–344. https://doi.org/10.1002/JPLN.201900402

Shi, M., Fisher, J. B., Brzostek, E. R., & Phillips, R. P. (2016). Carbon cost of plant nitrogen acquisition: Global carbon cycle impact from an improved plant nitrogen cycle in the community land model. *Global Change Biology*, *22*(3), 1299–1314. https://doi.org/10.1111/gcb.13131

Shi, M., Fisher, J. B., Phillips, R. P., & Brzostek, E. R. (2019). Neglecting plant–microbe symbioses leads to underestimation of modeled climate impacts. *Biogeosciences*, *16*(2), 457–465. https://doi.org/10.5194/bg-16-457-2019

Sitch, S., Friedlingstein, P., Gruber, N., Jones, S. D., Murray-Tortarolo, G., Ahlström, A., et al. (2015). Recent trends and drivers of regional sources and sinks of carbon dioxide. *Biogeosciences*, *12*(3), 653–679. https://doi.org/10.5194/BG-12-653-2015

Soudzilovskaia, N. A., van Bodegom, P. M., Terrer, C., Zelfde, M., McCallum, I., Luke McCormack, M., et al. (2019). Global mycorrhizal plant distribution linked to terrestrial carbon stocks. *Nature Communications*, *10*(1), 5077. https://doi.org/10.1038/s41467-019-13019-2

Sousa, D., Fisher, J. B., Galvan, F. R., Pavlick, R. P., Cordell, S., Giambelluca, T. W., et al. (2021). Tree canopies reflect mycorrhizal composition. *Geophysical Research Letters*, *48*(10), e2021GL092764. https://doi.org/10.1029/2021GL092764

Steidinger, B. S., Crowther, T. W., Liang, J., Van Nuland, M. E., Werner, G. D. A., Reich, P. B., et al. (2019). Climatic controls of decomposition drive the global biogeography of forest-tree symbioses. *Nature*, *569*(7756), 404–408. https://doi.org/10.1038/s41586-019-1128-0

Sterner, R. W., & Elser, J. J. (2002). *Ecological stoichiometry: The biology of elements from molecules to the biosphere*. Princeton University Press. https://doi.org/10.2307/j.ctt1jktrp3

Sullivan, B. W., Smith, W. K., Townsend, A. R., Nasto, M. K., Reed, S. C., Chazdon, R. L., & Cleveland, C. C. (2014). Spatially robust estimates of biological nitrogen (N) fixation imply substantial human alteration of the tropical N cycle. *Proceedings of the National Academy of Sciences of the United States of America*, *111*(22), 8101–8106. https://doi.org/10.1073/PNAS.1320646111

Sulman, B. N., Brzostek, E. R., Medici, C., Shevliakova, E., Menge, D. N. L., & Phillips, R. P. (2017). Feedbacks between plant N demand and rhizosphere priming depend on type of mycorrhizal association. *Ecology Letters*, *20*(8), 1043–1053. https://doi.org/10.1111/ele.12802

Sulman, B. N., Salmon, V. G., Iversen, C. M., Breen, A. L., Yuan, F., & Thornton, P. E. (2021). Integrating arctic plant functional types in a land surface model using above- and belowground field observations. *Journal of Advances in Modeling Earth Systems*, *13*(4), e2020MS002396. https://doi.org/10.1029/2020MS002396

Sulman, B. N., Shevliakova, E., Brzostek, E. R., Kivlin, S. N., Malyshev, S., Menge, D. N. L., & Zhang, X. (2019). Diverse mycorrhizal associations enhance terrestrial C storage in a global model. *Global Biogeochemical Cycles*, *33*(4), 501–523. https://doi.org/10.1029/2018GB005973

Sun, Y., Goll, D. S., Ciais, P., Peng, S., Margalef, O., Asensio, D., et al. (2020). Spatial pattern and environmental drivers of acid phosphatase activity in Europe. *Frontiers in Big Data*, *2*, 51. https://doi.org/10.3389/FDATA.2019.00051

Sun, Y., Peng, S., Goll, D. S., Ciais, P., Guenet, B., Guimberteau, M., et al. (2017). Diagnosing phosphorus limitations in natural terrestrial ecosystems in carbon cycle models. *Earth's Future*, *5*(7), 730–749. https://doi.org/10.1002/2016EF000472

Swaty, R., Michael, H. M., Deckert, R., & Gehring, C. A. (2016). Mapping the potential mycorrhizal associations of the conterminous United States of America. *Fungal Ecology*, *24*, 139–147. https://doi.org/10.1016/j.funeco.2016.05.005

Tanga, J., & Riley, W. J. (2018). Predicted land carbon dynamics are strongly dependent on the numerical coupling of nitrogen mobilizing and immobilizing processes: A demonstration with the E3SM land model. *Earth Interactions*, *22*(11), 1–18. https://doi.org/10.1175/EI-D-17-0023.1

Terrer, C., Jackson, R. B., Prentice, I. C., Keenan, T. F., Kaiser, C., Vicca, S., et al. (2019). Nitrogen and phosphorus constrain the CO_2 fertilization of global plant biomass. *Nature Climate Change*, *9*(9), 684–689. https://doi.org/10.1038/s41558-019-0545-2

Terrer, C., Vicca, S., Hungate, B. A., Phillips, R. P., & Prentice, I. C. (2016). Mycorrhizal association as a primary control of the CO_2 fertilization effect. *Science*, *353*(6294), 72–74. https://doi.org/10.1126/science.aaf4610

Terrer, C., Vicca, S., Stocker, B. D., Hungate, B. A., Phillips, R. P., Reich, P. B., et al. (2018). Ecosystem responses to elevated CO_2 governed by plant-soil interactions and the cost of nitrogen acquisition. *New Phytologist*, *217*(2), 507–522. https://doi.org/10.1111/nph.14872

Thornton, P. E., & Rosenbloom, N. A. (2005). Ecosystem model spin-up: Estimating steady state conditions in a coupled terrestrial carbon and nitrogen cycle model. *Ecological Modelling*, *189*(1–2), 25–48. https://doi.org/10.1016/J.ECOLMODEL.2005.04.008

Thum, T., Caldararu, S., Engel, J., Kern, M., Pallandt, M., Schnur, R., et al. (2019). A new model of the coupled carbon, nitrogen, and phosphorus cycles in the terrestrial biosphere (QUINCY v1.0; revision 1996). *Geoscientific Model Development*, *12*(11), 4781–4802. https://doi.org/10.5194/gmd-12-4781-2019

Todd-Brown, K. E. O., Randerson, J. T., Post, W. M., Hoffman, F. M., Tarnocai, C., Schuur, E. A. G., & Allison, S. D. (2013). Causes of variation in soil carbon simulations from CMIP5 Earth system models and comparison with observations. *Biogeosciences*, *10*(3), 1717–1736. https://doi.org/10.5194/bg-10-1717-2013

Turner, B. L., Brenes-Arguedas, T., & Condit, R. (2018). Pervasive phosphorus limitation of tree species but not communities in tropical forests. *Nature*, *555*(7696), 367–370. https://doi.org/10.1038/nature25789

van der Heijden, M. G. A., Martin, F. M., Selosse, M.-A., & Sanders, I. R. (2015). Mycorrhizal ecology and evolution: The past, the present, and the future. *New Phytologist*, *205*(4), 1406–1423. https://doi.org/10.1111/nph.13288

Vitousek, P. M., Cassman, K., Cleveland, C., Crews, T., Field, C. B., Grimm, N. B., et al. (2002). Towards an ecological understanding of biological nitrogen fixation. In *Biogeochemistry* (Vol. 57–58, pp. 1–45). Springer. https://doi.org/10.1023/A:1015798428743

Vitousek, P. M., & Field, C. B. (1999). Ecosystem constraints to symbiotic nitrogen fixers: A simple model and its implications. *Biogeochemistry*, *46*(1–3), 179–202. https://doi.org/10.1007/BF01007579

Vitousek, P. M., & Howarth, R. W. (1991). Nitrogen limitation on land and in the sea: How can it occur? *Biogeochemistry*, *13*(2), 87–115. https://doi.org/10.1007/BF00002772

Walker, A. P., Beckerman, A. P., Gu, L., Kattge, J., Cernusak, L. A., Domingues, T. F., et al. (2014). The relationship of leaf photosynthetic traits–V_{cmax} and J_{max}–To leaf nitrogen, leaf phosphorus, and specific leaf area: A meta-analysis and modeling study. *Ecology and Evolution*, *4*(16), 3218–3235. https://doi.org/10.1002/ece3.1173

Wang, Y. P., Houlton, B. Z., & Field, C. B. (2007). A model of biogeochemical cycles of carbon, nitrogen, and phosphorus including symbiotic nitrogen fixation and phosphatase production. *Global Biogeochemical Cycles*, *21*(1). https://doi.org/10.1029/2006GB002797

Wang, Y. P., Kowalczyk, E., Leuning, R., Abramowitz, G., Raupach, M. R., Pak, B., et al. (2011). Diagnosing errors in a land surface model (CABLE) in the time and frequency domains. *Journal of Geophysical Research*, *116*(G1), 1034. https://doi.org/10.1029/2010JG001385

Wang, Y. P., Law, R. M., & Pak, B. (2010). A global model of carbon, nitrogen and phosphorus cycles for the terrestrial biosphere. *Biogeosciences*, *7*(7), 2261–2282. https://doi.org/10.5194/bg-7-2261-2010

Waring, B. G., Adams, R., Branco, S., & Powers, J. S. (2016). Scale-dependent variation in nitrogen cycling and soil fungal communities along gradients of forest composition and age in regenerating tropical dry forests. *New Phytologist*, *209*(2), 845–854. https://doi.org/10.1111/nph.13654

Wieder, W. R., Butterfield, Z., Lindsay, K., Lombardozzi, D. L., & Keppel-Aleks, G. (2021). Interannual and seasonal drivers of carbon cycle variability represented by the community Earth system model (CESM2). *Global Biogeochemical Cycles*, *35*(9), e2021GB007034. https://doi.org/10.1029/2021GB007034

Wieder, W. R., Cleveland, C. C., Smith, W. K., & Todd-Brown, K. (2015a). Future productivity and carbon storage limited by terrestrial nutrient availability. *Nature Geoscience*, *8*(6), 441–444. https://doi.org/10.1038/ngeo2413

Wieder, W. R., Cleveland, C. C., Smith, W. K., & Todd-Brown, K. (2015b). Reply to "Land unlikely to become large carbon source". *Nature Geoscience*, *8*(12), 893–894. https://doi.org/10.1038/ngeo2606

Wieder, W. R., Lawrence, D. M., Fisher, R. A., Bonan, G. B., Cheng, S. J., Goodale, C. L., et al. (2019). Beyond static benchmarking: Using experimental manipulations to evaluate land model assumptions. *Global Biogeochemical Cycles*, *33*(10), 1289–1309. https://doi.org/10.1029/2018GB006141

Wullschleger, S. D., Epstein, H. E., Box, E. O., Euskirchen, E. S., Goswami, S., Iversen, C. M., et al. (2014). Plant functional types in Earth system models: Past experiences and future directions for application of dynamic vegetation models in high-latitude ecosystems. *Annals of Botany*, *114*(1), 1–16. https://doi.org/10.1093/aob/mcu077

Yang, X., & Post, W. M. (2011). Phosphorus transformations as a function of pedogenesis: A synthesis of soil phosphorus data using hedley fractionation method. *Biogeosciences*, *8*(10), 2907–2916. https://doi.org/10.5194/BG-8-2907-2011

Yang, X., Post, W. M., Thornton, P. E., & Jain, A. (2013). The distribution of soil phosphorus for global biogeochemical modeling. *Biogeosciences*, *10*(4), 2525–2537. https://doi.org/10.5194/bg-10-2525-2013

Yang, X., Post, W. M., Thornton, P. E., & Jain, A. K. (2014). *Global gridded soil phosphorus distribution maps at 0.5-degree resolution*. Oak Ridge National Laboratory Distributed Active Archive Center. https://doi.org/10.3334/ORNLDAAC/1223

Yang, X., Ricciuto, D. M., Thornton, P. E., Shi, X., Xu, M., Hoffman, F., & Norby, R. J. (2019). The effects of phosphorus cycle dynamics on carbon sources and sinks in the Amazon region: A modeling study using ELM v1. *Journal of Geophysical Research: Biogeosciences*, *124*(12), 3686–3698. https://doi.org/10.1029/2019JG005082

Yang, X., Thornton, P. E., Ricciuto, D. M., & Hoffman, F. M. (2016). Phosphorus feedbacks constraining tropical ecosystem responses to changes in atmospheric CO_2 and climate. *Geophysical Research Letters*, *43*(13), 7205–7214. https://doi.org/10.1002/2016GL069241

Yang, X., Thornton, P. E., Ricciuto, D. M., & Post, W. M. (2014). The role of phosphorus dynamics in tropical forests–A modeling study using CLM-CNP. *Biogeosciences*, *11*(6), 1667–1681. https://doi.org/10.5194/bg-11-1667-2014

Zaehle, S., Friedlingstein, P., & Friend, A. D. (2010). Terrestrial nitrogen feedbacks may accelerate future climate change. *Geophysical Research Letters*, *37*(1). https://doi.org/10.1029/2009gl041345

Zaehle, S., Jones, C. D., Houlton, B., Lamarque, J. F., & Robertson, E. (2015). Nitrogen availability reduces CMIP5 projections of twenty-first-century land carbon uptake. *Journal of Climate*, *28*(6), 2494–2511. https://doi.org/10.1175/JCLI-D-13-00776.1

Zhang, Y., Song, C., Band, L. E., & Sun, G. (2019). No proportional increase of terrestrial gross carbon sequestration from the greening Earth. *Journal of Geophysical Research: Biogeosciences*, *124*(8), 2018JG004917. https://doi.org/10.1029/2018JG004917

Zhao, M., Heinsch, F. A., Nemani, R. R., & Running, S. W. (2005). Improvements of the MODIS terrestrial gross and net primary production global data set. *Remote Sensing of Environment*, *95*(2), 164–176. https://doi.org/10.1016/j.rse.2004.12.011

Zhu, Q., Riley, W. J., Tang, J., Collier, N., Hoffman, F. M., Yang, X., & Bisht, G. (2019). Representing nitrogen, phosphorus, and carbon interactions in the E3SM land model: Development and global benchmarking. *Journal of Advances in Modeling Earth Systems*, *11*(7), 2238–2258. https://doi.org/10.1029/2018MS001571